Environmental drivers constraining the seasonal variability of satellite-observed and modelled methane at Northern high latitudes

Ella Kivimäki[1], Maria Tenkanen[2], Tuula Aalto[2], Michael Buchwitz[3], Kari Luojus[1], Jouni Pulliainen[1], Kimmo Rautiainen[1], Oliver Schneising[3], Anu-Maija Sundström[1], Johanna Tamminen[1], Aki Tsuruta[2], and Hannakaisa Lindqvist[4]

[1]Space and Earth Observation Centre, Finnish Meteorological Institute, Helsinki, Finland
[2]Climate Research, Finnish Meteorological Institute, Helsinki, Finland
[3]Institute of Environmental Physics (IUP), University of Bremen, Bremen, Germany
[4]Space and Earth Observation Centre, Finnish Meteorological Institute, Sodankylä, Finland

Correspondence: E. Kivimäki (ella.kivimaki@fmi.fi)

Abstract. Methane emissions from Northern high-latitude wetlands are associated with large uncertainties, especially in the rapidly warming climate. Satellite observations of column-averaged methane concentrations (XCH_4) in the atmosphere exhibit variability due to time-varying sources and sinks, and atmospheric transport. In this study, we investigate how environmental variables, such as temperature, soil moisture, snow cover, and the hydroxyl radical (OH) sink of methane, explain the seasonal variability of column-averaged methane concentrations (XCH_4) observed from space over Northern high-latitude wetland areas. We use XCH_4 data obtained from the TROPOMI instrument aboard the Sentinel-5 Precursor satellite, retrieved using the Weighting Function Modified Differential Optical Absorption Spectroscopy (WFMD) algorithm. In addition, we performed the analysis using two atmospheric inversion model configurations: one based on non-optimized prior fluxes, and another using fluxes optimized with in situ atmospheric observations. The aim was to assess the consistency between satellite-based and model-based results, and to explore differences in how environmental variables drive the variability of XCH_4.

Environmental variables are derived primarily from meteorological reanalysis datasets, with satellite-based data used for snow cover and soil freeze-thaw dynamics, and modeled modelled data for the OH sink. Our analysis focuses on five wetland-dominated case study regions over Northern high latitudes, including two in Finland and three in Russian Siberia, covering the period from 2018 to 2023.

Our findings reveal that environmental variables have a systematic impact on satellite-based XCH_4 variability: the seasonal variability is most strongly influenced by snow cover and soil water volume. Seasonal variability is primarily driven by the OH sink and snow, particularly snow water equivalent, while daily variability is primarily affected by soil temperature. Our most strongly affected by air temperature. The results are largely consistent with in-situ-based local studies but, although the role of snow is more pronounced . Our results demonstrate how satellite appears more pronounced in our analysis. We observe interesting differences in the environmental drivers influencing satellite-based and model-based XCH_4. The posterior results after in-situ data assimilation were better aligned with the satellite-based results than the prior, suggesting that while there remains room for improvement in model priors and configurations, there is already some consistency between the modeled

and observed total-column methane dynamics. However, the prior fluxes used in the model could benefit from improved snow information.

25   Overall, our results demonstrate how satellite-based XCH_4 observations can be used to study the seasonal variability of atmospheric methane over large wetland regions. The results imply that satellite observations of atmospheric composition, along with other Earth Observations as well as meteorological reanalysis data, can be jointly informative of the processes controlling the emissions in Northern high latitudes.

1

30   Methane (CH_4) is the second most important anthropogenic greenhouse gas (GHG), in terms of its total radiative forcing, following carbon dioxide (CO_2). In recent decades, methane concentrations in the atmosphere have experienced a rapid growth rate, the drivers of which are being debated (e.g.**??**). The highest growth rates were observed in 2020–2021, which have been explained by increased emissions from wetlands in both the tropics and high northern latitudes (**????**). Globally, approximately 65% of methane emissions are anthropogenic, with agriculture and waste management being the primary contributors ~~(**??**)~~(**??**)

35 . The main natural source is wetlands and inland freshwater systems. The main sink of methane is chemical loss by hydroxyl radicals (OH), primarily in the troposphere. According to ~~**??**~~ **??** 65% of the global emissions originate from south of 30°N, and methane emissions from high latitudes (north of 60°N) represent only 4% of the global total. However, uncertainties in the high-latitude regions are notably larger, with atmospheric measurement-based top-down estimates having uncertainties exceeding ~~±~~±20%, compared to less than ~~±~~±5% globally. Since 1979, the high Northern latitudes have been warming nearly

40 four times faster than the global average (**?**), a phenomenon with potentially significant consequences for methane emissions in these sensitive areas: for example, a warming climate can lead to an extended growing season or longer shoulder seasons, during which emissions are higher on a monthly basis, compared to colder months (**???**). Additionally, warming can directly increase methane emissions from specific land cover types (**?**) ~~,~~ or thaw permafrost, potentially leading to rising emissions~~: continuous permafrost regions, for instance, have shown lower emissions compared to discontinuous~~, since regions with less

45 permafrost have found to have lower methane fluxes compared to continuous permafrost regions (**??**).

    Seasonal variability in methane concentration in the Northern Hemisphere is driven by the seasonality of its sinks and sources, while in the Southern Hemisphere, the sink dominates (**?**). Although anthropogenic methane emissions show ~~some~~ in some sectors seasonal variability in the high latitudes (**?**), likely related to factors such as gas production or biomass burning (**?**), natural emissions show much stronger seasonal variability, mainly driven by wetland emissions (**??**). Methane emissions from

50 wetlands are influenced by wetland conditions and environmental variables, including, for example, temperature (**???**), soil moisture and water table level (**?**), and snow cover together with soil frost (**????**). The methane emissions from wetlands are primarily driven by anaerobic processes, where methanogens produce methane by reducing carbon dioxide with hydrogen or breaking down acetate (**?**). Such processes are sensitive to environmental conditions that can limit microbial activity, particularly through changes in water availability. Both overly dry and overly wet soils can reduce microbial activity, as

55 suitable moisture levels are required for microbial decomposition. Freezing of the soil, in particular, can limit the availability

of liquid water, slowing microbial processes. Furthermore, the main sink of methane, oxidation by OH radicals, has a strong seasonality driven by the number of OH radicals, which is influenced by seasonal variations in their production: OH is primarily produced by the photolysis of ozone in the presence of water vapor, and its concentration fluctuates with factors such as temperature, humidity, and UV radiation (**??**). These meteorological factors vary seasonally especially in the middle and high latitudes, leading to seasonal variation of the OH sink. Additionally, when considering methane concentrations throughout the atmosphere, transport must be accounted for due to methane's lifetime of approximately nine years ~~(?)~~(**?**). Transport patterns can affect the seasonal variability of methane over long time scales, and changes in transport patterns and emissions in other regions might influence observed concentrations elsewhere (**?**).

~~Methane concentrations~~ The seasonal variability of methane have often been studied using in situ measurements and models. In situ measurements can accurately measure the methane concentration or flux at a single point close to the ground or in a tower. Their advantage lies in their high accuracy and continuous time series, allowing the use of a network of stations for precise calculations of the regional or global methane budget. However, gaps in the measurement network hamper the precise localization of emissions and the results are difficult to extrapolate to larger areas. This is because in situ flux measurements often represent specific conditions, such as particular land cover, vegetation type, soil humidity, and local climate. Additionally, these measurements require electricity and access to the measurement site and, therefore, the flux measurements are often limited to the thaw and snow-free seasons due to maintenance reasons. Models, on the other hand, can describe large-scale phenomena, but they require comprehensive observations to model processes accurately.

The use of satellites in GHG studies has been possible since the 2000s. Satellite observations of methane concentrations in the near-infrared wavelengths started in 2002, when SCIAMACHY onboard Envisat was launched (**?**). The Greenhouse Gases Observing Satellite (GOSAT), launched in 2009, was the first satellite dedicated to GHG observations (**?**), followed by the TROPOspheric Monitoring Instrument (TROPOMI) onboard the Copernicus Sentinel-5 Precursor satellite in 2017. In addition to these missions, small satellites such as GHGSat also measure methane concentrations, but their utility for large-scale analysis is limited due to their narrow swath and infrequent revisit times. From SCIAMACHY to TROPOMI, both spatial and temporal resolutions have significantly improved; for example, pixel sizes have decreased from tens of kilometres to a few kilometres, and revisit times have reduced from several days to one day.

Satellites observe column-averaged dry-air mole fraction of methane (XCH_4), which is retrieved from solar radiation in the near-infrared wavelengths reflected by the atmosphere or ground surface. Therefore, satellite observations of methane are dependent on sunlight. At high latitudes, the lack of sunlight causes a so-called winter gap in GHG satellite observations, as measurements cannot be conducted due to the sun being close to or beyond the horizon. In addition to large solar zenith angles, cloud cover presents challenges for retrieval algorithms. Additionally, surfaces with a spectrally dependent reflectance, such as snow cover (**?**), can introduce retrieval errors (**?**). Despite these factors that limit data availability in the Northern high latitudes, updated and improved retrieval algorithms and the high spatial coverage of TROPOMI have reduced the length of the winter data gap at high latitudes. For the latest version of Weighting Function Modified Differential Optical Absorption Spectroscopy retrievals (WFMD v1.8; **??**), the observational coverage is, in principle, gapless when considering areas above 50$°°$N overall (**?**). Satellite observations of methane have been used in a wide range of studies, for example, to identify the location and

intensity of local point sources (**??**), as well as to investigate variations in methane trends (**??**). Additionally, methane satellite retrievals have been widely utilized to inform inversion models on methane concentrations (**???**)(e.g., **???**).

In this study, we investigate how environmental variables explain the seasonal variability of satellite-observed column-averaged methane concentrations over high-latitude wetland areas. As shown by **?**, the seasonal methane cycle in the Northern Hemisphere remains poorly understood due to gaps in wetland emission inventories. Satellite observations of methane concentrations can offer a more detailed view, both spatially and temporally, of the processes shaping this cycle in high northern wetlands. Our aim is to determine how environmental variables, related to methane emissions, together with methane loss by OH, influence total-column concentrations. Based on the in situ measurement findings presented above, we focus particularly on the roles of temperature, soil moisture, snow cover, soil freeze and thaw, and the impact of the OH sink, while also examining whether our results align with these in situ findings. We concentrate on high-latitude wetland areas because, as shown by **?**, ensemble forward model runs are not always able to accurately reproduce the seasonal methane cycle in the Northern Hemisphere due to incomplete wetland emission inventories. Satellite observations of methane would be valuable in complementing inversion results, as they could provide new insights that help reduce uncertainties in the global methane budget and ultimately improve our understanding of the increasing and varying methane trend In addition, we assess the consistency of satellite-based results and those from an atmospheric inverse model optimized with in-situ measurements of methane. The purpose is to compare the variability of column-averaged methane concentrations as driven by the environmental variables. The model simulations are performed using the CarbonTracker Europe – CH_4 (CTE-CH_4, **?**) system, and include two configurations: (1) a forward simulation using prior (non-optimized) fluxes, and (2) an inversion simulation in which fluxes have been optimized using in situ atmospheric observations. In Section 2, we introduce the datasets used, followed by the methods in Sect. 3. Section 4 presents and discussed the results and the conclusions are presented in Sect. 6.

2 Data sets

2.1 TROPOMI WFMD XCH$_4$ product

The TROPOspheric Monitoring Instrument (TROPOMI) on board the Copernicus Sentinel-5 Precursor (S5P) satellite was launched in October 2017 and it is dedicated to produce observations for air quality and climate monitoring. With its wide swath of approximately 2600 km, a daily global coverage can be attained. Currently, two retrieval algorithms are generated to retrieve the column-averaged dry-air mole fraction of methane (XCH_4) from the near-infrared spectra: the operational TROPOMI XCH_4 product, developed by the SRON Netherlands Institute for Space Research (**??**), and the Weighting Function Modified Differential Optical Absorption Spectroscopy (WFMD) algorithm, developed by the University of Bremen (**??**). In this study, we use XCH_4 concentrations retrieved by the WFMD algorithm due to its accuracy and suitability for our analysis. The WFMD v1.8 product shows no seasonal bias when comparing to high-latitude ground-based observations and AirCore data, resulting in lower mean bias and standard deviation (**?**). Furthermore, the WFMD product provides significantly more data from high Northern latitudes, particularly during the spring months, and features a shorter winter gap.

The WFMD algorithm retrieves simultaneously the column-averaged dry-air mole fractions of CH_4 and carbon monoxide (CO). The WFMD algorithm employs a linear least-squares retrieval which uses scaling or shifting of pre-selected atmospheric vertical profiles. The linearised radiative transfer model is fitted to the measured sun-normalised radiance to obtain the vertical columns of CH_4 and CO. The retrieval uses look-up tables for fast solutions and accounts for a range of typical atmospheric conditions, e.g., different solar zenith angles, surface albedos, and temperatures. The latest version of WFMD, version 1.8, includes significant changes compared to the previous version aimed at improving retrieval performance for different spectral albedos and updating the digital elevation model to reduce bias associated with topography, especially at high latitudes (??). In addition, the quality filter was refined in the post-processing, which improved cloud filtering over the Arctic. The improvement was particularly pronounced for water areas in the Arctic, but the precision of the cloud-free classification for land observations also increased significantly. At the time of writing of this paper, WFMD

2.2 Atmospheric inverse model CTE-CH$_4$

CarbonTracker Europe - CH_4 (CTE-CH$_4$; ?) is a global atmospheric inverse model that estimates surface methane fluxes by optimising scaling factors for prior emissions using an ensemble Kalman filter (??). The model setup follows ?, but uses updated prior fluxes and atmospheric in-situ observation datasets. Methane fluxes are optimised weekly at $1°\times1°$ resolution over Europe, Russia, Canada, and the USA, and regionally elsewhere. Spatial correlation lengths are set to 100 km in $1°\times1°$ regions, 500 km in coarser land areas, and 900 km over oceans. Anthropogenic and wetland fluxes are optimised independently but simultaneously; other sources (fires, termites, ocean, geological) remain fixed to their prior estimates. The prior anthropogenic fluxes are taken from GAINS (?) for the European Union, Norway, Switzerland, and the United Kingdom, and from EDGAR v8 (?) elsewhere. Wetland priors are based on JSBACH-HIMMELI (??) in Europe (12°W–37°E, 35°N–73°N) and LPX-Bern DYPTOP v1.8 is the latest available retrieval version..4 (???) elsewhere, both including peatland and mineral soil fluxes as well as soil sinks. Biomass burning fluxes are from GFEDv4.1s (?), excluding agricultural waste burning to avoid overlap with anthropogenic priors. Termite, ocean, and geological fluxes follow published estimates (???), with geological fluxes downscaled to a global total of 21 Tg yr^{-1}. All prior fluxes were monthly averages and anthropogenic, wetland and biomass burning fluxes varied from year to year. Since LPX-Bern DYPTOP provides estimates only until 2019, we used the 2010–2019 average for 2020–2022. Prior uncertainties are set to 80% for terrestrial and 20% for oceanic sources, assumed uncorrelated. We use an ensemble size of 500, a 5-week fixed lag, and prior uncertainties of 80% for terrestrial and 20% for oceanic fluxes, assuming no correlation between land and ocean, following ? and ?.

The TM5 transport model (?) is used as the observation operator. It runs globally at $6°\times4°$ resolution, with nested zooms including a $1°\times1°$ domain over Europe (21°W–45°E, 24°N–74°N) and a $3°\times2°$ buffer (36°W–54°E, 14°N–82°N). The model has 25 hybrid sigma-pressure levels and is driven by 3-hourly ECMWF ERA5 meteorology (?). It includes monthly-varying atmospheric sinks from reactions with OH, Cl, and O(^{1}D) (???), without interannual variability (see also Sect. 2.7 for OH sinks). Simulated mole fractions are compared to in situ observations from the Integrated Carbon Observation System, the National Oceanic and Atmospheric Administration ObsPack (v4.0 in 2018–2020 and v7.0 in 2021–2022) (??), and the Finnish Meteorological Institute (Kumpula, Sodankylä). The dataset includes weekly discrete samples and hourly continuous measurements,

which are averaged to daily means. Site-specific uncertainties (4.5–75 ppb) account for both measurement accuracy and representativeness errors. Measurements differing by more than three times their uncertainty from modelled values are excluded during assimilation to minimise biases from unresolved local sources or meteorological mismatches.

2.3 IMS Daily Northern Hemisphere Snow and Ice Analysis product

Interactive Multisensor Snow and Ice Mapping System (IMS) snow cover and sea ice analysis products from the U.S. National Ice Center (USNIC) are derived from a variety of different data sources, including satellite images and in situ observations. The daily data set is available since February 1997 and it is produced in three different spatial resolutions: 1 km, 4 km, and 24 km. The data have a four-class classification method for a surface refarding snow and ice: open water, land without snow, sea or lake ice, and snow-covered land.

In our analysis, we used only data over land, i.e. land without snow and snow-covered land classes. We used the 24 km resolution data version for the time period from 2018 to 2023 (**?**).

2.4 The Copernicus Global Land Monitoring Service Snow Water Equivalent product

The Copernicus Global Land Service Snow Water Equivalent (SWE) product provides daily estimates of the equivalent amount of liquid water stored in the snowpack across the Northern Hemisphere, with a spatial resolution of 5 km (**??**). Snow presence is identified using optical satellite observations, while SWE values are derived through assimilation of passive microwave satellite data and snow depth measurements. Areas covered by lakes, sea ice, mountains, glaciers, and permanent ice are excluded from the dataset. The daily dataset is available since January 2006 and is updated in near real-time.

To describe the amount of snow in our case study regions we used SWE data from 2018 to 2023.

2.5 SMOS Level 3 Soil Freeze and Thaw product

The European Space Agency's (ESA) Soil Moisture and Ocean Salinity (SMOS) Soil Freeze and Thaw (F/T) product provides an operational satellite-derived, Level 3 soil freeze and thaw state dataset across the Northern Hemisphere (**??**). The observations from the SMOS satellite, primarily designed to measure soil moisture over land and surface salinity over oceans, are the basis for the F/T product. This dataset is generated by the Finnish Meteorological Institute using SMOS Level 3 gridded brightness temperature data provided by the Centre Aval de Traitement des Données SMOS (CATDS) (**??**).

The processing algorithm for the SMOS F/T product integrates two auxiliary datasets, 2-meter air temperature and snow cover data, to refine the accuracy of the freeze-thaw classifications and mitigate obvious misclassifications. The soil state is categorized into three levels: frozen, partially frozen, and thawed soil.

The product covers the time period from 2010 to the present, with daily operational updates available at a latency of approximately one day, ensuring its relevance for ongoing research and applications. The data resolution is 25 km $\times$ 25 km, structured on the Equal-Area Scalable Earth (EASE2) grid. For this study, we utilized SMOS v3 data for the years 2019–2023, focusing on ascending orbit data, as these are less affected by radio frequency interference (RFI) over the Eurasian continent

? compared to the descending orbits. Since late 2022, the war in Ukraine has significantly increased RFI, particularly over Europe, leading to a substantial reduction in usable data in 2023. This has affected the analysis and results presented in this paper.

2.6 ERA5 reanalysis data

The European Centre for Medium-Range Weather Forecasts (ECMWF) produces the ERA5 reanalysis, which is widely used as a global meteorologica dataset for scientific purposes (**?**). ERA5 provides large data sets of variables related to atmosphere, ocean-waves and land-surface quantities. Reanalysis is a scientific method where the global past observations are integrated into a current advanced computer models, allowing the reconstruction of past atmospheric or land conditions globally, even over areas without in situ observations. ERA5 is based on Integrated Forecasting System (IFS) and is therefore primarily an atmospheric model, but it is coupled with a land surface model and a wave model to estimate land and ocean parameters. ERA5 Land (**?**) variables are generated using advanced data assimilation techniques that integrate various observations to provide accurate and high-resolution land surface data. The horizontal resolution of ERA5 is 31 km and there are 137 vertical layers and the current hourly data on single levels cover time the period from 1940 to present. For the public reanalysis product, the data have been regridded for $0.25° \times 0.25°$ regular grid. ERA5 is widely used for meteorological research and has been developed since 1950.

For this study, we used hourly data on single levels from 2018 to 2023 (**?**). The obtained variables were 2m temperature, soil temperature and volumetric soil water at Layer 1. Layer 1 represents the soil depth between 0–7 cm, where the surface is located at 0 cm. In the model, the 2m temperature is calculated by interpolating between the lowest model level and the Earth's surface. Soil temperature represents the temperature at the middle of the layer, calculated by estimating heat transfer between the layers. The soil water volume takes into account soil texture and classification, soil depth, and the underlying groundwater level (**?**).

2.7 CH_4 loss by OH radicals

The tropospheric OH concentrations were estimated based on **?**, but scaled by 0.92 globally following the optimized estimates using methyl chloroform data (**??**)(**??**). The stratospheric OH loss was calculated based on **?**. The CH_4 loss based on the OH fields was calculated using the global Eulerian atmospheric chemistry transport model TM5 (**?**). TM5 was run at the resolution of $6° \times 4°$ (latitude x longitude) x 25 vertical levels globally constrained by 3-hourly interpolated ECMWF ERA5 meteorological fields, and using posterior CH_4 fluxes from CTE-CH_4 (**??**)(**?**) produced for the Global Methane Budget (**?**). The chemical reactions were calculated off-line, such that the prescribed monthly climatological OH fields and reaction rates were used in the simulation. The monthly total OH losses were calculated for the entire latitude zone 57°N–70°N. Note the TM5 setups here differ slightly from those used to derive CTE-CH4 concentrations (Section 2.2).
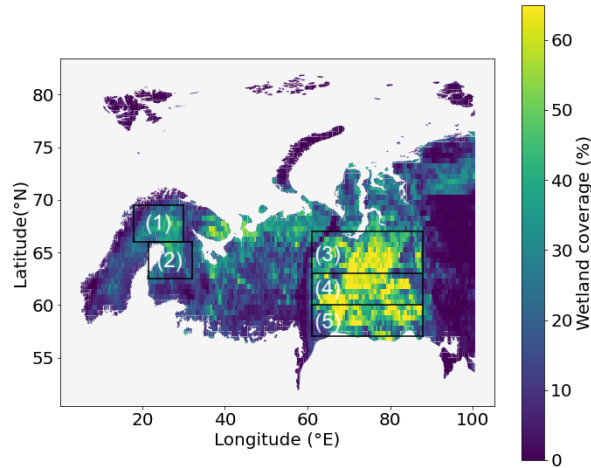
Figure 1. Northern Finland (1), Southern Finland (2), Northern Siberia (3), Middle Siberia (4) and Southern Siberia (5) case study areas marked over BAWLD total wetland coverage map.

3 Methods

The methods used to define the case study areas, process the data sets, and study the links between the environmental variables and the variability of XCH_4 are described as follows. First, the case study areas were defined based on wetland data. Next, the gap filling process and the fitting of the seasonal cycle to the XCH_4 time series are explained. The methods for gridding and averaging environmental variables to align them with the XCH_4 time series are then outlined. Finally, the application of random forest ~~feature importance and permutation importance to study~~ importance methods and partial dependence plots, used to investigate the connections between the time series ~~are described.~~

, is described.

3.1 Defining the case study areas

To investigate how environmental variables explain the seasonal variability of XCH_4 over Northern high latitude wetland areas, we needed to define case study regions that are both representative of wetland areas and exhibit seasonality in environmental variables. A general challenge in defining a case study area, is that one hand it has to be large enough to host a sufficiently representative set of concentration observations but on the other hand small enough so that the area is to some extent homogeneous when considering the emissions and sinks. ~~After testing, we decided to concentrate on five areas over the Northern Eurasia~~We tested different case study areas over Canada and Eurasia based on inversion results of natural methane fluxes (e.g., **??**) and wetland coverage from the The Boreal-Arctic Wetland and Lake Dataset (BAWLD, **?**). We selected five areas in Northern Eurasia, with sufficient spatiotemporal coverage of TROPOMI data to constrain the fit for the XCH_4 seasonal cycles and perform further analysis. The areas are shown in Fig. 1 and are called Northern Finland, Southern Finland, Northern Siberia,

Table 1. Total wetland fraction and three most significant wetland types in the five case study regions based on BAWLD wetland data (**?**). In some of the regions, there are also other wetland types. Therefore, the total fraction does not necessarily match the sum of the three types listed here.

	Total wetland (%)	Bog (%)	Permafrost bog (%)	Fen(%)
~~Northern Finland~~ Northern Finland (66–69.5°N, 18–30°E)	26.5	11.2	0.4	13.8
~~Southern Finland~~ Southern Finland (62.5–66°N, 21.5–32°E)	23.3	12.6	0.0	10.0
~~Northern Siberia~~ Northern Siberia (63–67°N, 61–88°E)	40.2	5.5	19.1	8.8
~~Middle Siberia~~ Middle Siberia (60–63°N, 61–88°E)	45.8	20.8	1.2	19.7
~~Southern Siberia~~ Southern Siberia (57–60°N, 61–88°E)	40.8	21.0	0.0	16.9

Middle Siberia, and Southern Siberia. The borders of the case study areas were defined based on ~~The Boreal-Arctic Wetland and Lake Dataset (BAWLD , ?)~~ BAWLD dataset. Figure 1 shows the case study areas over BAWLD total wetland fraction map. In addition, the latitude and longitude borders of the areas are listed in Table 1. The total wetland and wetland type fractions for each case study area are also listed in Table 1. Based on the map in Fig. 1 and Table 1, for the Siberian case study areas, the total wetland fraction is over 40% and for the Finnish case study areas it is over 20%. The main wetland type is fen for Northern Finland, and bog for Southern Finland and Middle and Southern Siberia. Northern Siberia is the only area where permafrost bog is the main wetland type and also where the permafrost bog fraction is significant. The border between the Northern and Middle Siberia case study regions was defined in such a way that it separates areas where permafrost bog or bog is the dominant bog type.

3.2 ~~Time series gap filling and fitting~~ Comparison of ~~the seasonal cycle of~~ satellite-based XCH$_4$ to model-based XCH$_4$

~~(a) TROPOMI WFMD daily median XCH$_4$ (blue dots), gap-filled XCH$_4$ values (grey dots) and fitted seasonal cycle and trend, and their uncertainties (red and shaded red) for Middle Siberia. (b) shows the same for the detrended time series.~~

~~Before applying gap filling and fitting the seasonal cycle of XCH$_4$~~ Before applying any time series analysis, we collected all quality-flagged TROPOMI/WFMD v1.8 data for each case study ~~area~~ region, covering the period from January 2018 to ~~April 2024.~~ December 2023. To enable comparison between satellite-retrieved column-averaged methane and model-based estimates, each satellite observation was first co-located with the corresponding model grid cell. The modelled XCH$_4$ values were then calculated using the satellite averaging kernel, following the formulation by **?**:

$$XCH_{4,\text{mod}} = \sum_l \left(X_{\text{apr}}^l + A^l \left(X_{\text{mod}}^l - X_{\text{apr}}^l \right) \right) w^l, \tag{1}$$

where A^l is the satellite averaging kernel, X^lapr is the prior methane profile used in the retrieval, X^lmod is the modelled methane profile, and w^l is the pressure-based weighting function for layer l. The modelled methane profiles were linearly interpolated from the model vertical levels to the satellite retrieval levels using the logarithm of the pressure profiles. For each day, we ~~calculated~~ computed the regional daily median XCH$_4$ ~~, along with its standard deviation and the number of observations~~
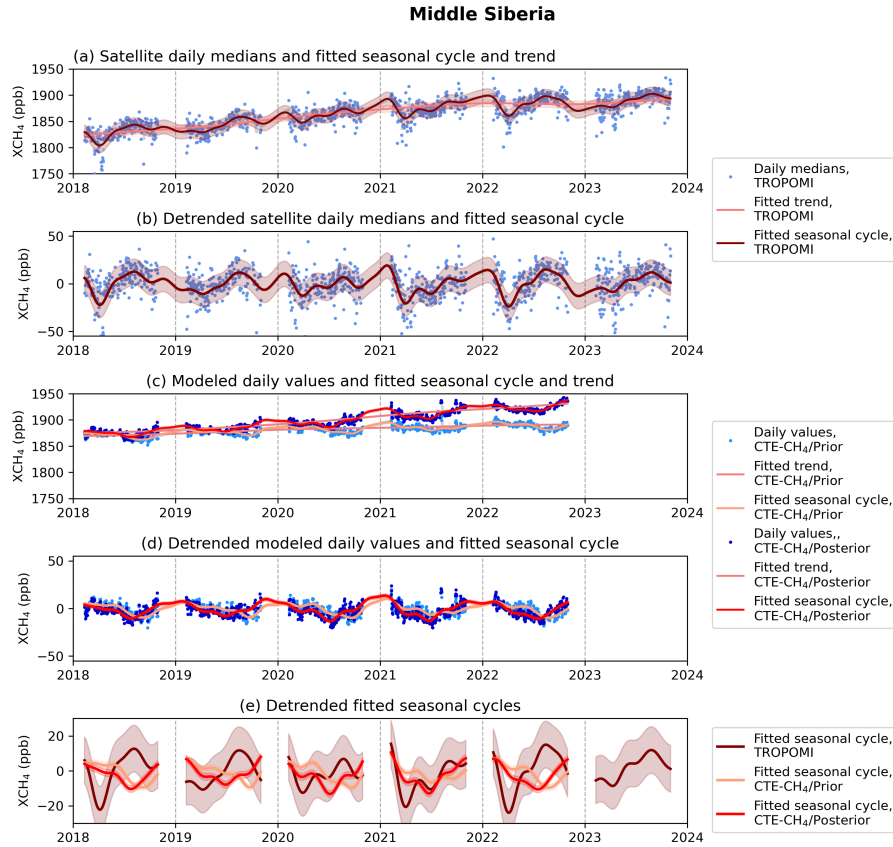
Figure 2. (a) TROPOMI/WFMD daily median XCH$_4$ values (blue dots) with the fitted seasonal cycle and trend, including their uncertainties (red and shaded red), for Middle Siberia. (b) Same as (a), but detrended TROPOMI/WFMD XCH$_4$ time series. (c) CTE-CH$_4$/Prior and Posterior daily XCH$_4$ values (lighter and darker blue dots, respectively), along with the fitted seasonal cycle and trend, and their uncertainties (lighter and darker red lines, and corresponding shaded areas). (d) Same as (c), but detrended CTE-CH$_4$ time series. (e) Detrended fitted seasonal cycles and their uncertainties for TROPOMI/WFMD and CTE-CH$_4$/Prior and Posterior XCH$_4$.

per day, based on all observations within for both the satellite observations and the model estimates. Due to the relatively large grid cell size of CTE-CH$_4$ (6° longitude × 4° latitude), and because the WFMD prior profile is similar within each region, the modelled XCH$_4$ values were very similar across one region and the variations were mainly caused by the averaging kernels of the area for that day. To minimize the influence of potential outliers, the daily median was calculated only for days with more than three observations. This restriction excluded a few individual spring dates. TROPOMI/WFMD observations.

3.3 Time series gap filling and fitting of the seasonal cycle of XCH$_4$

After calculating the daily mediansvalues, we applied a Kalman filter for gap filling the data for the fitting, and the seasonal cycle was fitted using NOAA's curve fitting routine (CCGCRV; **??**). CCGCRV is a non-linear fitting routine, developed by **?** to

smooth and separate the seasonal cycle and long-term trend~~of CO₂ from the Mauna Loa in situ measurements~~. CCGCRV fits the long-term trend with third order polynomial function and the seasonal cycle is modelled with harmonic functions;

$$y = a_0 + a_1 x + a_2 x^2 + \sum_{n=1}^{4} [a_{2n+1} \sin(2n\pi x) + a_{2n+2} \cos(2n\pi x)] \tag{2}$$

where the terms a_0, a_1, a_2 represent the trend components, while the summation term captures the seasonal variation through the sine and cosine functions. The function is fitted with linear least squares regression routine that also gives the covariance of the fitting parameters and therefore the uncertainty of the parameters estimated. The fitting process produces a constant seasonal cycle, and to account for interannual and short-term variations, the residuals are filtered (**??**). CCGCRV gives as output the fitted trend, harmonic seasonal cycle with no interannual variability and smoothed seasonal cycle, where the interannual and short term variations are included. When considering the seasonal cycle of methane, CCGCRV has been previously used, for example, to study the decreasing seasonal cycle of methane in the Northern high latitudes (**?**) and the year-to-year anomalies of satellite observations of methane in tropical wetlands (**?**).

The fit for each individual day in the CCGCRV method can be described as a combination of the function fit, which represents the harmonic cycle without interannual variability, and the filtered residuals, which accounts for interannual and short-term variations. Similarly, the uncertainty of each component can be estimated by combining the variances of these different elements (**?**). For example, the uncertainty of the smoothed seasonal cycle is calculated by combining the variances of the function fit and the residual filter:

$$\sigma^2_{\text{smooth}} = \sigma^2_{\text{function}} + \sigma^2_{\text{filter}}. \tag{3}$$

Likewise, the uncertainty of the trend can be determined by combining the variances of the polynomial fit and the filter (**?**).

? investigated the possible biases related to three different curve fitting programs, CCGCRV being one of them. **?** concluded and generated general recommendations on the use of these curve fitting programs and their suitability for time series analysis. Based on these recommendations, we considered CCGCRV suitable for our analysis, as it was recommended to in cases where the year-to-year anomalies or the magnitude or timing of the seasonal cycle are studied.

To avoid the limitations of CCGCRV related to missing observations, it was suggested by **?** that the data are gap-filled before applying CCGCRV, as CCGCRV only interpolates over the gaps.

We experimented different gap filling methods and studied their effect on the seasonal cycle in the Middle Siberia. The methods tested included the interpolation that CCGCRV can perform on its own, as well as Kalman filtering. For the Kalman filter, we experimented with several different parameter settings. Based on our analysis, the timing and the shape of the harmonic cycle fitted by Eq. (2) were quite similar regardless of the gap-filling method, for the time outside the winter gap in the satellite data. The main differences in the fitted cycles were related to the amplitude of the seasonal cycle, as the winter maximum often coincided with a winter data gap, and the timing of this maximum also varied slightly between fits. Based on our tests, we decided to use the Kalman filter for gap filling, as it initially provided the lowest chi-squared values for the function fit and the smallest residual standard deviation. The Kalman filter settings were further optimized to minimize the chi-squared value and the residual standard deviation although the differences between these metrics were small and varied slightly

between the model and the satellite data, and case study area. The finalized Kalman filter configuration was kept consistent across all case study areas and for both the satellite and model datasets. ~~The defined Kalman filter settings were kept similar for each case study area.~~ For the analysis, the winter gap was excluded to avoid drawing conclusions from periods without observations. ~~This, along with the effect and contribution of the gap-filling method on the results, is discussed in Sect. 4.~~

After filling ~~the~~ data gaps using the Kalman filter, we applied CCGCRV to the gap-filled time series for each study region, ~~and~~ both for satellite-based and model-based XCH_4. We then calculated the uncertainties ~~of~~ associated with the smoothed seasonal cycles derived from the fitted curves. Figure 2 shows an example of the XCH_4 daily ~~medians, gap-filled values,~~ values and the fitted smoothed seasonal ~~cycle with its uncertainty, and the fitted trend~~ cycles, including their uncertainty estimates, as well as the fitted trends for Middle Siberia, based on both satellite and model data. Similar figures for other case study areas can be found in Appendix B, specifically in Figs. B1, B2, B3, and B4.

To investigate the spring time seasonal minima and maxima of the satellite-based XCH_4 seasonal cycle in relation to factors such as snowmelt, we needed to determine the dates of these minima and maxima, along with their uncertainty estimates. To calculate the uncertainty estimates, we utilized the fitted harmonic seasonal cycle and the parameters a_n provided by the CCGCRV fit (as shown in Eq. (2)), along with the uncertainty estimates derived from the covariance matrix using a Monte Carlo approach. We sampled 10,000 states of the fitted cycle and calculated the dates of the minima and maxima for each state using the find_peaks function from the Python scipy.signal package. For each minimum and maximum, we computed the standard deviation across these 10,000 states and used these standard deviations as the uncertainty estimates for the results presented in Sect. 4. The distribution of the values around each individual minimum and maximum was found to be Gaussian, allowing us to use the computed standard deviation for each minimum and maximum reliably as an uncertainty estimate. This analysis was not applied to the modelled XCH_4 seasonal cycles, as their temporal behavior did not allow for a consistent investigation of these features across regions.

3.4 Gridding and averaging of environmental variables

As environmental datasets in this study, we used the SMOS freeze/thaw state (F/T), IMS snow state (snow), The Copernicus Global Land Service Snow Water Equivalent product (SWE), ERA 2 m temperature (T/2m), ERA5 soil temperature at layer 1 (T/soil), ERA5 volumetric soil water at layer 1 (soil W) and CH_4 loss by OH (OH). These datasets are described in detail in Sect. 2, where, for example, the spatial and temporal resolutions are provided for each dataset. Abbreviations in parentheses corresponding to the variable names used in Sect. 4.

All environmental data were initially collected for the case study areas, presented in Sect. 3.1, and daily mean values along with their standard deviations were calculated over the areas. ~~The~~ There was no need to gap fill the environmental data sets ~~were not gap filled~~, as they consist of daily time series. Variations in the temporal and spatial resolution of the datasets required slight adjustments in averaging methods. SMOS F/T and IMS snow cover are categorical datasets: SMOS F/T has three categories, while IMS has two. For SMOS, we defined frozen as 1, partially frozen as 0.5, and thawed soil as 0. We then averaged these values across each case study area to obtain the regional mean soil freeze-thaw state. In the IMS snow cover data, snow-covered areas were defined as 1 and snow-free areas as 0, which allowed us to calculate the average snow cover fraction for each area.
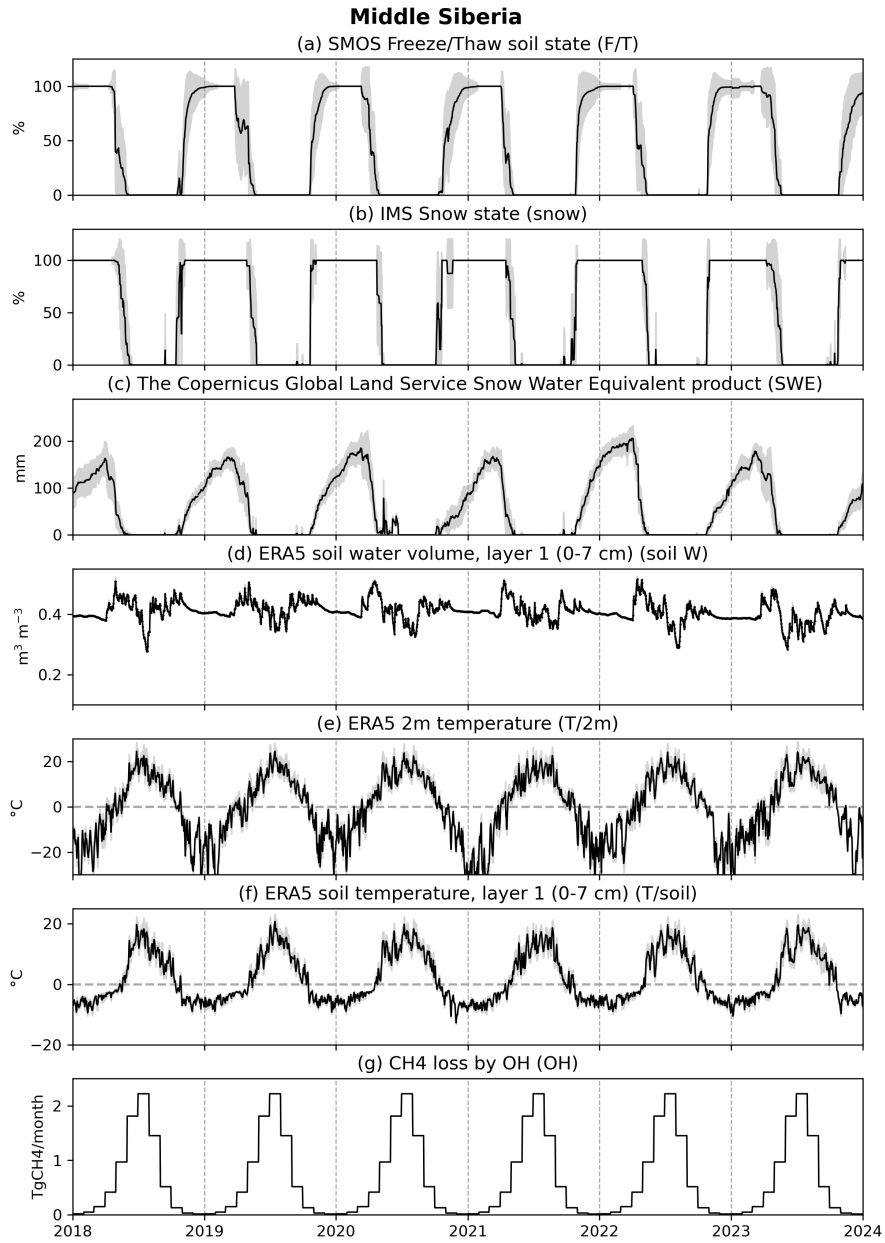
Figure 3. Black line shows the daily mean and the filled grey area the standard deviation of (a) soil freeze-thaw state, (b) snow cover state, (c) snow water equivalent, (d) layer 1 soil water volume, (e) 2 meter air temperature, (f) layer 1 soil temperature and (g) CH_4 loss by OH for Middle Siberia. The abbreviation mentioned in parentheses in the title of each subfigure is the abbreviation to be used for that environmental variable in the results.

Snow water equivalent data has a daily temporal resolution, allowing us to calculate daily area-averaged values directly. For temperatures and soil water volume, derived from the ERA5 reanalysis data, hourly means were first calculated for each area, and from these hourly means, daily average temperatures and their standard deviations were computed. For the CH_4 loss by OH, there is no variability between years or a within month, as it has already been calculated for the 57°N–70°N latitude band, making it consistent regardless of the study area or year. Figure 3 illustrates the environmental time series for Middle Siberia. Similar figures for other case study areas can be found in Appendix C, specifically in Figs. C1, C2, C3, and C4.

The environmental datasets have relatively coarse spatial resolution, with the smallest grid cell size being 5 km in the SWE data and the largest being approximately 27.8 km in the ERA5 data along the longitude direction. The environmental variables in this case, such as snow cover or temperature, can vary significantly within these grid cells, depending on factors such as land type. For example, a transition from forest to wetland within a grid cell can lead to substantial variation in the variables. Therefore, in addition to the variability of environmental variables within the case study area, it is important to consider that there may also be variability within the grid cells.

For seasonal timing comparison (Sect. 4.2), we required estimates of the start and end dates of snow cover melt and beginning of decreasing SWE, along with their uncertainties. We defined the start of snow cover melt as the date when the IMS snow state over the area was below 0.9, and snow cover was considered completely melted when the mean snow cover fell below 0.1. To estimate uncertainties for these dates, we examined when the mean snow cover $\pm 1\sigma$ uncertainty fell below 0.9 for melt onset and below 0.1 for complete melt. This approach provided uncertainty bounds in both directions for the start and end dates of snow cover melt. To obtain the date when SWE begins to decrease significantly, we normalized the SWE data for each study area for each winter and identified the first day in spring when the normalized SWE was below 0.75; this day was used to represent the beginning of SWE decline. The uncertainties for this timing were estimated similarly to those for snow cover melt, by identifying the days when the mean SWE $\pm 1\sigma$ uncertainty dropped below 0.75.

3.5 Random forest feature importance and permutation importance

To study the links between the environmental variables and variability of XCH_4 on the daily level, we applied ~~random forest~~ the random forest (RF) regression method, using two different importance metrics~~:~~, random forest feature importance (RFFI) and permutation importance (PI) methods, within the random forest model. Here, the environmental variables act as features in the random forest, allowing us to assess their individual contributions to XCH_4 variability. In addition, we used partial dependence plots (PDPs) to illustrate how the RF model predicts the XCH_4 concentrations as a function of a single environmental variable. PDPs can provide detailed insight into the relationship between individual environmental drivers and XCH_4.

In general, random forest is a robust and well-established ensemble learning method that averages multiple decision trees to avoid overfitting and ~~to improve the accuracy of the results~~ improve accuracy (**?**). RFFI and PI are importance metrics that can be used to evaluate the relationship between environmental variables and the seasonal variability of XCH_4. RFFI measures variable importance based on tree structure, while PI evaluates it by shuffling values within the variable, assessing the resulting impact on model performance. By analysing these scores together with PDPs, we can study the connections of environmental

variables and seasonal variability XCH$_4$ in more detail. The scores provide different types of information, and the calculated importance values can either support each other or highlight some differences.

The first importance method, RFFI, measures how each variable contributes to the decision-making process within the random forest model. RFFI is normalized to provide a relative ranking of variable importance so that the sum of importance values over the variables is one. The second method, PI, describes the performance of the model when the values of each environmental variable are shuffled. PI directly measures the impact of each environmental variable on the random forest model's predictive accuracy, which provides additional information about the relevance of each environmental variable by showing how much the prediction error increases when a particular variable is disrupted. It is important to note that the calculated RFFI and PI importance values are not directly comparable as they measure different aspects and their units are different. Using both methods together allows for a more comprehensive understanding of variable importance by comparing the effects of different importance methods and settings on the results.

Additionally, high correlations between environmental variables can influence the RFFI results, as highly correlated variables may share importance, making it difficult to distinguish their individual contributions. In contrast, PI is less sensitive to correlations as it measures the independent impact of each variable on model performance, although it may still be affected by shared information in cases of strong correlations. For this reason, using both importance methods is advisable, as environmental variables are often correlated. The PDPs allow us to assess how each environmental variable contributes to the model's predictions. However, when interpreting PDPs, it is important to note that they may yield unrealistic results for strongly correlated variables, as the model may evaluate data combinations that do not occur in reality. Among the environmental variables that we use in our analysis, the following were highly (i.e., correlation coefficient $|r| \geq 0.85$) correlated: snow cover and snow water equivalent ($r = 0.89$), snow cover and soil freeze-thaw state ($r = 0.91$), snow cover and soil temperature ($r = -0.85$), snow water equivalent and soil freeze-thaw state ($r = 0.96$), 2 meter air temperature and soil temperature ($r = 0.93$), and soil temperature and OH ($r = 0.86$). These high correlations can mostly be explained by physical mechanisms and are not surprising. It is important to take these correlations into account, especially when interpreting the RFFI results, but also when evaluating the PDPs.

The random forest model performance requires a large data volume; therefore, we collected data from all of the case study regions. For the XCH$_4$ satellite observations, the number of daily median values from all regions combined was 5,399, whereas for the modelled XCH$_4$ data, the number of daily values was 4,435. This difference is due to the fact that the modelled data ends in the end of 2022, while the satellite time series continues until the end of 2023. The regional distribution of daily values for TROPOMI and CTE-CH$_4$ data, respectively, was as follows: Northern Finland: 818 and 676; Southern Finland: 820 and 675; Northern Siberia: 1,201 and 993; Middle Siberia: 1,218 and 1,001; Southern Siberia: 1,342 and 1,090.

We studied separately the relationship of environmental variables and the fitted seasonal cycle of XCH$_4$ (e.g., Fig. 2(b) red line), and the relationship of environmental variables and detrended daily XCH$_4$ values (e.g., Fig. 2(b) blue dots)

estimate the ~~,~~ using both satellite and model data. The aim was to identify potentially different drivers ~~for the variability in~~ of variability at different time scales. For both ~~, we conducted the same methods:~~ the seasonal cycle and the daily values, we used only those days when we had TROPOMI XCH$_4$ observations~~were considered~~. Therefore, the analysis and results can be considered to apply only to the spring-summer-fall period as we are missing XCH$_4$ values from winter time.

405 ~~To obtain the results of this study we~~ We used scikit-learn Python module and its built-in methods and functions for fitting the model and to calculate RFFI and PI (**?**). The random forest model was set up with 100 decision trees and trained using 80% of the available data, with the remaining 20% used for testing the model's performance. The model was implemented without pruning. We tested different numbers of trees, but the model's performance did not significantly improve as the number of trees increased. Given the relatively small size of the dataset, it was important to keep the number of trees small enough.

410 For ~~the~~ permutation importance, we defined the number of repetitions to be 20 to obtain a robust estimate of each variable's contribution. The PDPs were also calculated using the pre-built method in scikit-learn and the brute-force approach, which generates predictions for modified input data to directly estimate the marginal effect of each variable. The brute-force method was used for its flexibility and compatibility with correlated variables and various model types.

For the results presented in Sect. ~~4.1~~4, the number of features to consider when determining the best split (parameter 415 'max_features') was set to 'sqrt', meaning the number of features considered at each split was the square root of the total number of features in the model. ~~The choice of 'max_features' was based on a sensitivity analysis that assessed model performance and root mean square error (RMSE) using cross-validation.~~ In addition to 'sqrt', we also tested with 'n_features', where all features are considered when determining the best split. The choice of the number of features had no effect on the ranking of the feature importances, indicating robust identification of key drivers regardless of the model configuration. Model 420 performance ~~improved slightly with 'sqrt', increasing the model's~~ was assessed by calculating the coefficient of determination (R^2) ~~from 0.840 to 0.851 for the seasonal cycle, and from 0.317 to 0.322 for daily medians. The RMSE decreased~~ and root mean square error (RMSE) using cross-validation. For each of the three XCH$_4$ data sets, R^2 and RMSE were slightly better with 'n_features' than with 'sqrt' for the seasonal cycle ~~from 8.05 ± 2.84 ppb to 7.93 ± 2.94 ppb, while it increased slightly for daily medians from 14.09 ± 1.21 ppb to 14.16 ± 1.17 ppb.~~ (e.g., for TROPOMI XCH$_4$, the mean R$^2 = 0.75 \pm 0.02$, RMSE 425 $= 4.33 \pm 0.13$ vs. R$^2 = 0.73 \pm 0.02$, RMSE $= 4.50 \pm 0.12$ over 1 000 Random Forest model iterations). However, for the daily medians, 'sqrt' produced either better or identical metrics compared to 'n_features' (e.g., for TROPOMI XCH$_4$, R$^2 = 0.28 \pm 0.03$, RMSE $= 14.00 \pm 0.37$ vs. R$^2 = 0.30 \pm 0.02$, RMSE $= 13.82 \pm 0.37$). Although the changes in performance metrics were small ~~when altering the 'max_features' parameter~~and the sensitivity analysis showed that the better-performing setting varied between the seasonal cycle and daily medians, 'sqrt' was chosen as the final configuration because it increases 430 tree diversity, reduces the risk of overfitting, and generally improves model generalization. ~~For permutation importance, we defined the number of reputations to be 50 to obtain a robust estimate of each variable's contribution.~~

To evaluate the uncertainty of RFFI and PI~~we fitted the random forest model~~, and to assess the robustness of the calculated feature importance values and rankings, we performed repeated training–test splits using 1000 ~~times using~~ different random seeds and Random Forest model iterations. The final feature importance values ~~that are~~ presented in the results in Sect. ~~4.1,~~ 4 435 were calculated as the average ~~of these thousand fits~~across these 1000 fits, and the uncertainties of the importance values were

estimated by calculating ~~the~~ their standard deviation. In addition, PDPs, presented in Sect. 4 were computed as the mean over 1000 RF model fits, and the uncertainties are calculated by taking the standard deviation of ~~the sample~~PDPs over those 1,000 fits.

~~Among the environmental variables that we use in our analysis, the following were highly (i.e. correlation coefficient $|r| \geq 0.85$) correlated: snow cover and snow water equivalent ($r = 0.89$), snow cover and soil freeze-thaw state ($r = 0.91$), snow cover and soil temperature ($r = -0.85$), snow water equivalent and soil freeze-thaw state ($r = 0.96$), 2 meter air temperature and soil temperature ($r = 0.93$), and soil temperature and OH ($r = 0.87$). These high correlations can mostly be explained by physical mechanisms and are not surprising. It is important take these correlations into account, especially when analysing the RFFI results~~In addition, to assess the consistency of the importance rankings, we performed a 10-fold cross-validation, repeating the entire procedure ten times with different random seeds. The final importance scores were calculated by averaging across all folds and repetitions to obtain robust estimates. The results calculated over the ten 10-fold cross-validation runs showed similar feature rankings compared to those obtained from the 1,000 random seed–based RFFI and PI results. The calculated mean importance scores were also largely consistent and fell mostly within the calculated standard deviation uncertainty ranges. Some variation was observed in individual 10-fold runs, particularly for the RFFI results, which is expected. As shown in Table A1, for example, the mean RFFI scores of four environmental variables influencing the satellite-based XCH_4 seasonal cycle fall within a narrow range of 0.11–0.13. Moreover, Fig. 4 illustrates the uncertainty ranges for the PI scores, indicating variability across the 1,000 random seed iterations.

4 Results~~and discussion~~

4.1 Links between environmental variables and XCH_4

~~The ranking of environmental variables based on their importance to XCH_4 variability. The height of each bar represents the variable's rank: a higher bar indicates greater importance. Each colour indicates different XCH_4 component (blue: daily median; red: fitted seasonal cycle; grey: daily median − seasonal cycle difference) and the shade of the colour the used importance method (darker: PI; lighter: RFFI).~~

~~Our aim is to study the links between environmental variables and the seasonal variability of~~ Figure 4 shows the PI scores of each of the studied environmental variables in explaining the variability of the detrended seasonal cycles of XCH_4 ~~and to estimate the potentially different drivers for the variability in different time scales. The time scales we consider include the fitted seasonal cycle~~ seasonal cycles and XCH_4 daily values. The results are shown separately for the satellite-based TROPOMI/WFMD, and the model-based CTE-CH$_4$/Prior and CTE-CH$_4$/Posterior. In addition to the visual representation in Fig. 4, Table A1 lists the mean importance scores calculated using both PI and RFFI methods over the 1,~~which captures the seasonal changes but cannot detect short-term variations or extremes,~~ 000 model iterations. Table A2, on the other hand, lists the rankings of the environmental variables based on their importance scores.

Based on Fig. 4, PI indicates that OH and SWE are the two most important environmental drivers of the XCH_4 seasonal cycle for both TROPOMI/WFMD v1.8 and ~~day-to-day variability, which is more sensitive to small-scale atmospheric changes~~
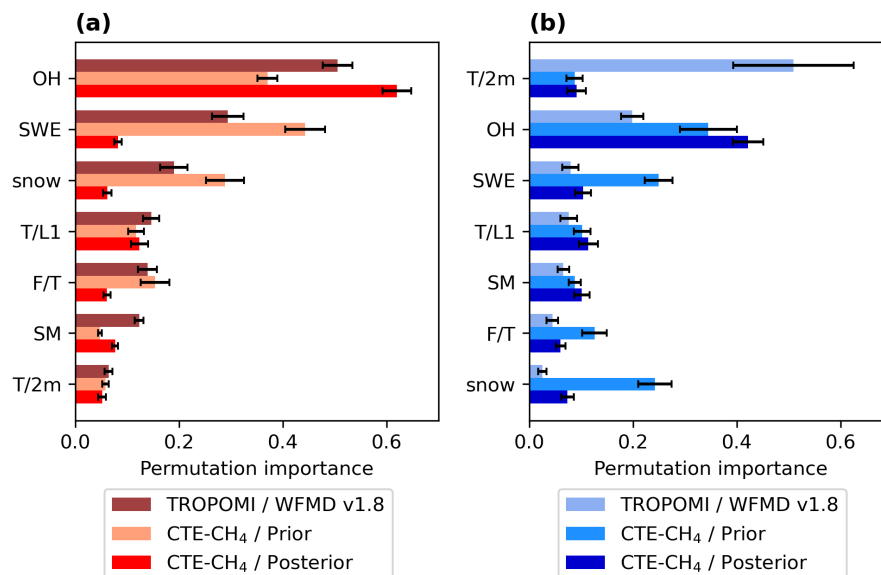
Figure 4. Permutation ~~and random forest feature~~ importance metrics for ~~XCH₄ seasonal cycle ((a)~~ XCH_4 seasonal cycles and (b) ~~),~~ XCH_4 daily ~~median ((c) and (d))~~values. Different colors represent TROPOMI/WFMD, ~~and XCHCTE-CH₄~~CTE-CH₄daily ~~median − seasonal cycle difference ((e) /~~Prior, and ~~(f)~~CTE-CH₄/Posterior. ~~The importances~~ Environmental variables are ordered ~~based on~~ according to the ~~permutation~~ TROPOMI/WFMD importance scores, ~~with~~ the most important ~~being~~ variable at the ~~uppermost~~ top and the ~~lowest being the~~ least important at the bottom. ~~The importances~~ Importance values are calculated as ~~an~~ the average ~~from 1000~~ of 1,000 random forest model fits, and the uncertainties (black lines) ~~are~~ represent the standard deviations ~~of those~~ across these fits.

470   ~~and can exhibit larger fluctuations than the seasonal cycle. In addition, we study the daily median − seasonal cycle difference,~~ ~~which describes how the daily value differs from~~ CTE-CH₄/Prior dataset. For TROPOMI, OH is the most important variable, followed by SWE. For CTE-CH₄/Prior, however, SWE ranks first and OH second. These results are consistent between PI and RFFI for TROPOMI (Table A2). For environmental variables unrelated to snow, the ranking varies substantially more between PI and RFFI in both TROPOMI and CTE-CH₄/Prior, although the importance scores of these variables are generally similar (Table A1). In contrast, the ~~seasonal value and is used in our analysis to strengthen the results; the daily median − seasonal cycle~~

475   ~~can be thought in a way as methane anomaly respect to the seasonal cycle. The methane~~ importance scores and rankings for the CTE-CH₄/Posterior dataset differ markedly from those of the other two XCH_4 seasonal cycles. OH is clearly the dominant driver in this case, while all other variables exhibit significantly lower importance scores, particularly in the PI results where the separation between OH and other variables is the most pronounced. The consistency of these findings is further supported by the overall performance of the random forest models. The mean coefficient of determination (R^2) for the XCH_4 ~~data used~~

480   ~~in this study (WFMDv.1.8) performs well compared to reference data sets across all seasons (?), indicating its reliability~~ ~~in capturing both seasonal and daily variability across all available time periods. The mean daily median − seasonal cycle~~ ~~difference varied between the case study areas, ranging from 2.0 ppb to 3.9 ppb. This difference is generally highest during~~

spring, when day-to-day variability peaks, with methane concentrations showing notably stronger low values on individual days (for example, Fig. 2 for the year 2018), and seasonal cycle is 0.73 for TROPOMI/WFMD, additionally, the concentration

485 drops sharply from the winter maximum to the winter minimum (0.89 for example, Fig. 2 for the year 2022) CTE-CH$_4$/Prior, and 0.84 for CTE-CH$_4$/Posterior. This indicates that seasonal variability is captured by the environmental variables selected in the three datasets.

For the daily values of XCH$_4$, both CTE-CH$_4$/Prior and CTE-CH$_4$/Posterior show that OH is the most important variable according to PI. However, for TROPOMI/WFMD, air temperature is the most important driver. Despite the relatively wide

490 uncertainty range associated with air temperature (Fig. 4), its dominant role is clearly evident and further supported by RFFI (Table A2). The ranking of environmental variables varies considerably between PI and RFFI for both CTE-CH$_4$/Prior and CTE-CH$_4$/Posterior. For example, while PI identifies OH as the most important driver in the CTE-CH$_4$/Prior case, RFFI ranks OH only sixth. Nevertheless, the mean coefficient of determination (R^2) for the XCH$_4$ daily values is 0.30 for TROPOMI/WFMD, 0.59 for CTE-CH$_4$/Prior, and 0.51 for CTE-CH$_4$/Posterior. These values are notably lower than those for

495 the XCH$_4$ seasonal cycle.

The analysis is performed by applying random forest regression method using RFFI and PI importance metrics. Figure 4 shows PI and RFFI of each studied environmental variable on the detrended

Figure 5 presents PDPs of the detrended seasonal cycle of XCH$_4$ daily medians ((a) and (b)), fitted , showing the modelled response of XCH$_4$ seasonal cycle ((c) and (d)) and for daily median – seasonal cycle difference ((e) and (f)). The environmental

500 variables are ordered in the y-axis based on their PI rankings. Black line shows the uncertainty of the importance. Figure ?? shows the ranking of environmental variables based on their importance to different variability to changes in each environmental variable. The results are shown separately for TROPOMI/WFMD, CTE-CH$_4$/Prior, and CTE-CH$_4$/Posterior. Figure 6 shows the corresponding PDPs for the detrended daily values of XCH$_4$. A decreasing line in the PDPs indicates that the RF model predicts lower XCH$_4$ components; the higher bar signifying higher significance. Each colour represents each values as the

505 environmental variable increases. Conversely, an increasing line suggests that XCH$_4$ component and the shade of the colour is based on the used importance method increases with the environmental variable. A steady line implies minimal dependency between the variable and the modelled XCH$_4$ response. When analysing the PDPs, it is important to focus on the shape and trends of the curves rather than absolute values, as these plots should be used to illustrate relative dependencies rather than quantitative predictions.

510 Based on Figs. 4 and ??, for the Overall, the partial dependence of TROPOMI/WFMD XCH$_4$ on the studied variables is closer to the dependence of CTE-CH$_4$/Posterior XCH$_4$ compared to CTE-CH$_4$/Prior. The partial dependence of seasonal cycle is the strongest with OH: OH exhibits a consistent negative relationship with XCH$_4$ for TROPOMI/WFMD and CTE-CH$_4$/Posterior. In contrast, the response of CTE-CH$_4$/Prior is more irregular and even anti-correlated with the predicted TROPOMI/WFMD XCH$_4$. The XCH$_4$ daily values have similar partial dependence on OH than the seasonal cycle, both PI and RFFI show

515 somehow similar patterns, SWE and soil water volume being the most important environmental variables. The order of importance for soil freeze-thaw state, air temperature , snow cover, soil temperature and OH varies slightly between PI and RFFI but all of these variables are less significant than SWE and soil moisture according to both methods but for TROPOMI/WFMD
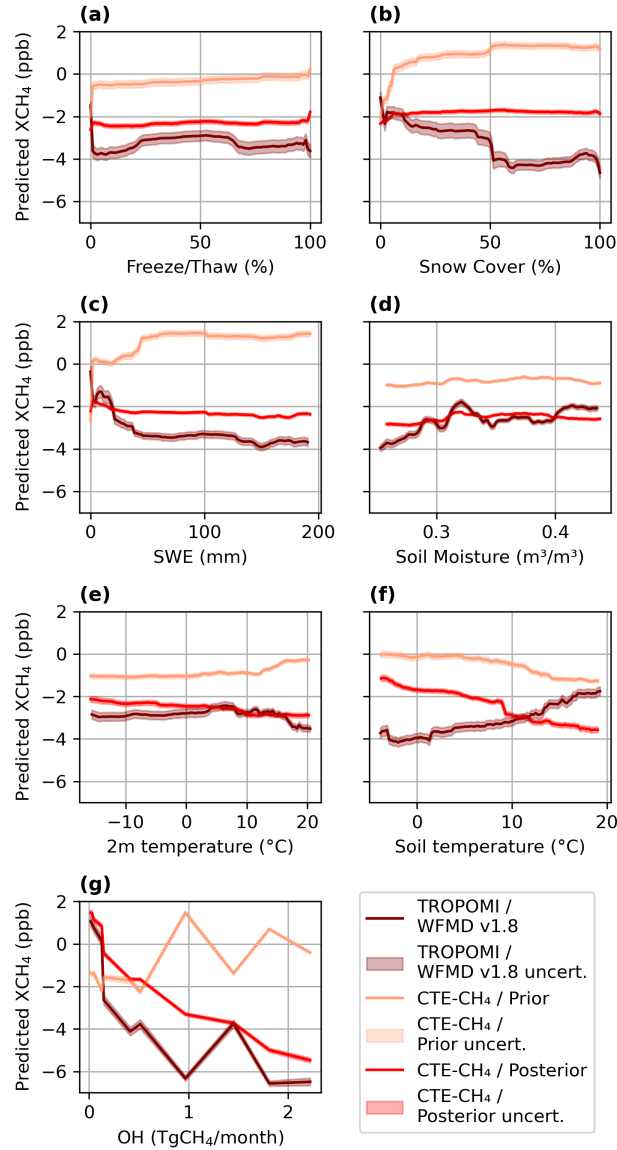
Figure 5. Partial dependence plots of the seasonal cycle of XCH_4. The red lines show the average RF model response to each environmental variable, calculated over 1,000 RF fits. Shaded areas represent the standard deviation across RF model runs, indicating the uncertainty of the partial dependence. The results are shown for three data sources (TROPOMI/WFMD, CTE-CH_4/Prior, and CTE-CH_4/Posterior), each plotted in different reds, with their corresponding uncertainties shown as shaded areas. Subplots illustrate the modelled partial dependence of XCH_4 seasonal cycle on (a) soil freeze–thaw state (F/T) (b) snow cover (snow), (c) snow water equivalent (SWE), (d) layer 1 soil moisture (SM), (e) 2 meter air temperature (T/2m), (f) layer 1 soil temperature (T/L1), and (g) CH_4 loss by OH (OH).
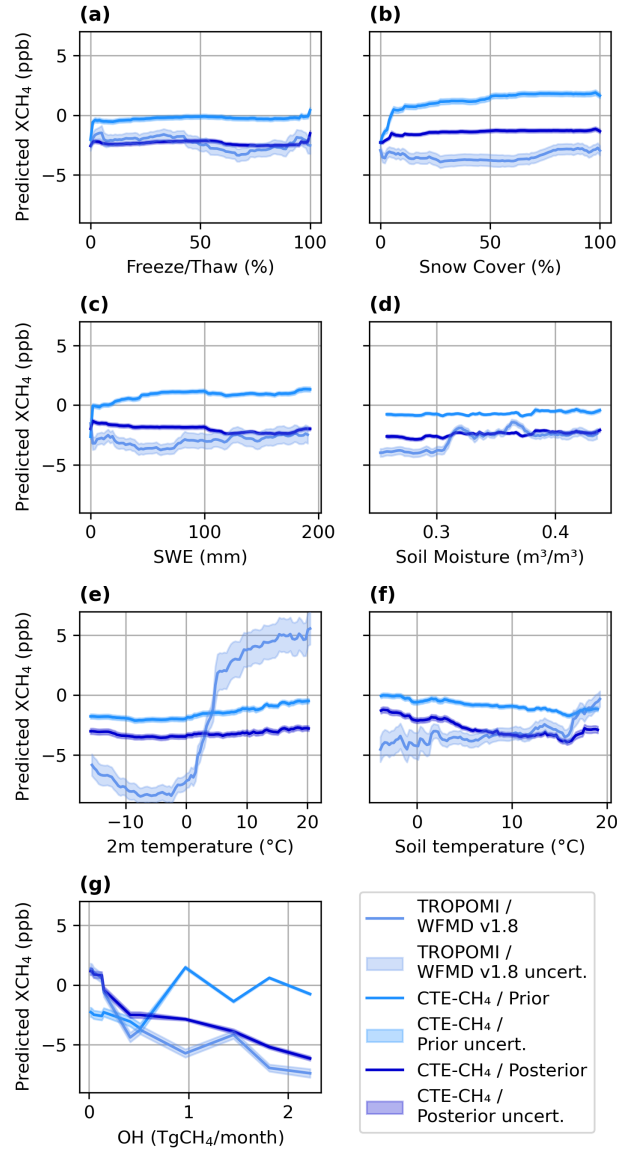
Figure 6. Partial dependence plots of the daily values of XCH$_4$. The blue lines show the average RF model response to each environmental variable, calculated over 1,000 RF fits. Shaded areas represent the standard deviation across RF model runs, indicating the uncertainty of the partial dependence. The results are shown for three data sources (TROPOMI/WFMD, CTE-CH$_4$/Prior, and CTE-CH$_4$/Posterior), each plotted in different blue, with their corresponding uncertainties shown as shaded areas. Subplots illustrate the modelled partial dependence of XCH$_4$ daily values on (a) soil freeze–thaw state (F/T) (b) snow cover (snow), (c) snow water equivalent (SWE), (d) layer 1 soil moisture (SM), (e) 2 meter air temperature (T/2m), (f) layer 1 soil temperature (T/L1), and (g) CH$_4$ loss by OH (OH).

XCH$_4$, air temperature has the most pronounced marginal effect. The model predicts a strong increase in XCH$_4$ as air temperature rises from 0°C to approximately 5°C, after which the response continues to increase but at a lower rate. For the

520   ~~XCH$_4$ daily medians and the difference between daily medians and the seasonal cycle, PI and RFFI produce somewhat similar results: according to both methods, soil temperature is the most important environmental variable for both XCH~~model-based daily values, the partial dependence on air temperature, as well as other variables, is relatively flat and indicates a minimal marginal effect. In addition to air temperature, the dependence on soil temperature in the model-based values, both seasonal cycle and daily, is opposite in direction compared to the satellite-based case. For TROPOMI/WFMD, the response is positive,

525   indicating that higher soil temperatures are associated with increased XCH$_4$~~variables. For PI, this is clearer than for RFFI,~~. In contrast, both CTE-CH$_4$/Prior and Posterior exhibit a negative dependence, suggesting a divergent behavior between satellite-based and ~~the order of importance for other environmental variables differs between the methods. Based on RFFI, OH is the second most important for~~ model-based seasonal cycles.

Snow water equivalent shows a strong relationship with the TROPOMI-based XCH$_4$ ~~daily medians, while based on PI, it~~

530   ~~is SWE. According to PI,~~ seasonal cycle for SWE values below 50mm, after which the response flattens. For CTE-CH$_4$/Prior, the ~~importance of other environmental variables than soil temperature and SWE are minimal, while based on RFFI, each environmental variable has some effect. For the daily median – seasonal cycle difference, soil temperature is the most important variable based on both RFFI and PI. This is somewhat expected, as soil temperature was not significant for the~~ relationship with SWE is increasing, such that higher SWE values are associated with higher XCH$_4$ ~~seasonal cycle, but it was for the daily~~

535   ~~medians, and SWE was important for both. Interestingly, for the difference, the soil water volume, which was a significant factor in~~ values, while CTE-CH$_4$/Posterior shows slight decreasing trend, similar to TROPOMI/WFMD. For TROPOMI/WFMD and CTE-CH$_4$/Prior, snow cover shows similar pattern than SWE but for CTE-CH$_4$/Posterior, it is almost flat.

In addition to seasonal cycles and daily values, we tested the capability of the ~~seasonal cycle, does not appear as an important variable for the daily median – seasonal cycle difference.~~ RF model to predict the daily value–seasonal cycle difference. The

540   coefficient of determination (R^2) for this difference was between 0.11–0.13 for all three datasets, indicating that only slightly over 10% of the variability in the difference could be explained with the RF model. As the R^2 values were this low, we did not perform an importance score analysis. While such an analysis could have indicated which of the environmental variables had the most significant contribution to the explained 10%, the overall explained variability was considered too limited for a meaningful interpretation. The mean daily value–seasonal cycle difference varied between case study areas, for TROPOMI/WFMD, the

545   range was –0.43 ppb to 0.29 ppb, for CTE-CH$_4$/Prior it was –0.04–0.9 ppb, and for CTE-CH$_4$/Posterior –0.01–0.16 ppb.
~~However,~~

4.2   Seasonal timing of XCH$_4$ minima and maxima in relation to snow

Our results in Sect. 4.1 demonstrated that snow-related variables, specifically snow water equivalent and snow cover, influence the ~~analysis also reveals that the RFFI results may not be as reliable for interpretation as those based on PI. As noted in~~

550   ~~Sect. 3.5, the correlation between environmental variables can affect their relative importance when considering RFFI, making it difficult to distinguish their individual contributions. This issue is particularly evident,~~ seasonal cycle of satellite-based
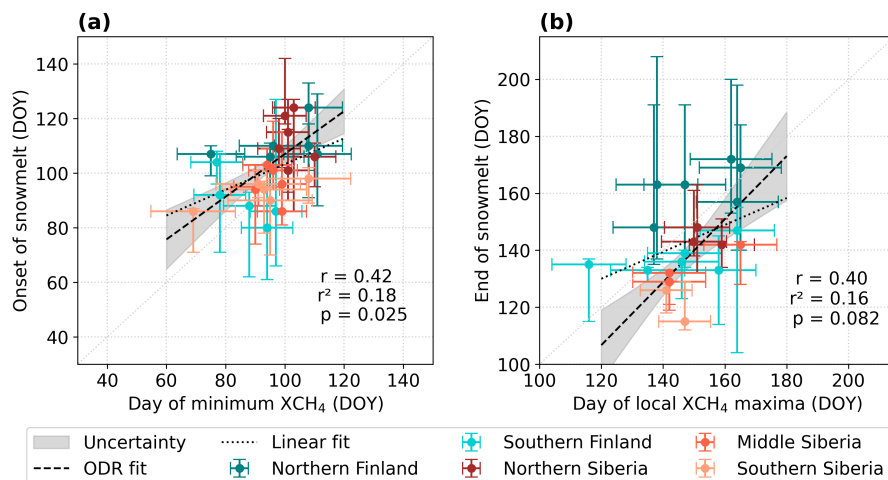
Figure 7. Scatter plots show (a) onset of snowmelt (y-axis) versus the day of the year when the XCH_4 seasonal cycle reaches its minimum (x-axis), and (b) the end of snowmelt (y-axis) versus the day of the local maxima in XCH_4 (x-axis). Both figures also display the one-to-one line in gray dots, a linear fit as a black dotted line, and an Orthogonal Distance Regression (ODR) fit as a black dashed line. The ODR fit accounts for uncertainties in both directions, with all uncertainties calculated based on the data. Additionally, the subplots display the Pearson correlation coefficient (r), the coefficient of determination (r^2), and the corresponding p-value.

XCH_4. To further investigate the temporal connection between snow and the seasonal cycle of XCH_4, we focused on spring, particularly on the minimum XCH_4 in early spring and the local maxima in late spring or early summer, coinciding with snowmelt. We focused on spring and not on the annual maximum because the annual maximum often coincides with a time when TROPOMI observations are not possible, due to polar night or low solar elevation (e.g., Fig. 2; see data gaps in winter 2021 and 2022). Additionally, the onset of snow cover frequently occurs during this period (Fig. D1), further complicating late-autumn or early-winter analyses. For the analysis, we defined the end of snowmelt based on snow cover, rather than SWE, because it is a simpler method for determination, and in SWE time series, it is observed that significant amounts of snow may still fall after SWE approaches zero, for example, in ~~the XCH_4 daily median results, where RFFI suggests that OH is the second most important variable, with an importance value very close to that of soil temperature~~ Fig. 3(c) in the spring of 2020. When determining the end of snowmelt based on snow cover, these situations were more precisely defined. The onset of snowmelt, however, must be defined through the start of SWE reduction, as SWE begins to decrease much earlier than snow cover (Fig. ~~4 (d)). In contrast, PI ranks OH as the third most important, with a clear difference in importance compared to soil temperature. According to correlation analysis, OH and soil temperature are highly correlated (r = 0.87) , which leads to challenges in distinguishing their individual importance in the RFFI results. Given these concerns, and considering the challenges RFFI faces when the features are correlated, we focus on the PI results and use RFFI results as supporting information for variables that are not as strongly correlated. It should also be noted that due to the high correlation of~~ D1), i.e. snowpack begins to melt

from the top before the ground becomes completely snow-free. Threshold-based methods for defining the onset and end of snowmelt are described in Sect. 3.4.

The seasonal cycle of XCH_4 generally reaches its minimum in early spring and its maximum during autumn or winter. In some years, particularly in the Finnish case study areas, local minima and maxima in XCH_4 are observed during late spring, often coinciding with snowmelt (Fig. D1). Figure 7 shows (a) the day of minimum XCH_4 relative to the onset of snowmelt, and (b) the day of a local maximum in XCH_4 compared to the end of snowmelt. In Fig. 7(a), the 2023 data point for Southern Finland is excluded because the XCH_4 minimum falls at the edge of the TROPOMI time series and is therefore not considered reliable. Both panels include a linear fit, represented by a dotted line, and an Orthogonal Distance Regression (ODR) fit, indicated by a dashed line. The ODR approach accounts for uncertainties in both the x and y directions. Both figures also display the Pearson correlation coefficient r, coefficient of determination r^2, and the corresponding p-value. Uncertainties related to the timing of snowmelt and the phase of the XCH_4 seasonal cycle are calculated as presented in detail in Sects. 3.3 and 3.4.

Based on Fig. 7(a), the onset of snowmelt shows a moderate positive correlation with the timing of the XCH_4 seasonal minimum, within uncertainties. When the potential outlier from the Southern Finland case study area in 2023 is excluded, as discussed earlier, the Pearson correlation coefficient r is 0.42. Including the outlier reduces the correlation to 0.32, highlighting the sensitivity of the result to individual data points given the small sample size (N = 30, covering six years and five case study areas). Nevertheless, with a p-value below 0.05, the relationship can be considered statistically significant, indicating a non-random association between snowmelt onset and XCH_4 minimum timing. In contrast, the correlation between the timing of the local XCH_4 maximum and the end of snowmelt is slightly weaker, with a Pearson correlation coefficient of 0.40. However, the associated p-value of 0.082 indicates that this relationship is not statistically significant at the 0.05 threshold. This analysis is further constrained by a smaller number of observations (N = 20, Fig. D1), increasing the influence of individual data points on the statistical outcome. The relationship between XCH_4 phase and snowmelt timing appears to be clearest in the Finnish case study areas, where a local maximum of XCH_4 occurs in conjunction with snowmelt every year studied. In Northern and Middle Siberia, this pattern is observed in three years, and in Southern Siberia, in two years, but the local maximum is less distinct there than in the Finnish areas. However, in Southern Siberia, even in those two years, the timing of the local XCH_4 maximum does not align with the end of snowmelt. In both cases, the slopes of the ODR and linear fits differ

similarly, reflecting the influence of uncertainty distribution and potential outliers. Overall, the ODR fits indicate that the onset of snowmelt tends to occur after the XCH$_4$ minimum, while the local XCH$_4$ maximum generally follows the end of snowmelt.

5   Discussion

5.1   Links between environmental variables and XCH$_4$

The driving factors and conditions of the seasonal variability of methane emissions from different land and vegetation types has been previously widely studied with in situ measurements ~~and~~ as well as modelled CH$_4$ fluxes and concentrations. As stated in the introduction, the seasonal variability of the column-averaged dry-air mole fraction of methane is a combination of the seasonality of CH$_4$ emissions and sinks, and atmospheric transport patterns. Therefore, the results from local flux studies cannot be directly compared to our findings, although fluxes influence the observed XCH$_4$ concentrations.

Next, we ~~will~~ compare our results with previous findings from in situ measurements and modelling studies and ~~model studies , and~~ examine how the dependencies of methane on environmental variables identified in those studies are reflected in our results. We will also discuss key differences between satellite and model-based results, with the aim of identifying similar patterns and discrepancies and possible reasons behind them. The comparison against CTE-CH$_4$/Prior concentrations provides insight into how well the prior fluxes, especially process-model based wetland CH$_4$ fluxes which are expected to be the main driver of the flux seasonality in the study regions, can reproduce the observed seasonal variability in total-column methane and its dependence on environmental drivers. In contrast, the posterior results assess the capability of surface-based inversion simulation to optimize and capture key features of the total column. In the inversion simulations, surface observations are used to optimize the posterior fluxes so that the model reproduces the observed surface concentrations. XCH$_4$ is then calculated from the modeled concentrations using these fluxes, and since part of the column variability originates higher in the atmosphere, the resulting total-column values can differ substantially from satellite-based XCH$_4$.

Role of the OH sink

? studied the hemispheric differences and the drivers of the seasonality of methane concentrations based on model simulations. They showed that in the Southern Hemisphere, the seasonal cycle is smooth and primarily driven by the OH sink~~but the seasonal cycle~~, whereas in the Northern Hemisphere, the cycle is asymmetric and ~~has~~ exhibits a sharp increase during summer. Based on their ~~results with~~ chemical transport model ~~, they found that~~the results, they concluded that, in addition to the role of OH, the magnitude, latitudinal distribution, and seasonality of wetland emissions are critical ~~for the seasonality~~ factors influencing the seasonal cycle of methane in the Northern Hemisphere, as they determine the timing and magnitude of the summer increase. ~~Our findings further specify those of ?, as our resultsprint out the importance of soil water volume, snow cover, and soil temperature; these variables are all important factors for methane production in high latitude wetlands, either directly or indirectly, by influencing the soil water cycle and temperature.~~ In our results, OH was identified as the most significant factor for the TROPOMI/WFMD and CTE-CH$_4$/Posterior XCH$_4$ seasonal cycles, based on both PI and RFFI scores. This

finding is consistent with **?** and demonstrates that, for total-column methane, atmospheric CH_4 loss is one of the key drivers of seasonal variability. For CTE-CH_4/Prior seasonal cycle, OH was the second most important factor. For daily values, there was a

635   clear difference between satellite-based and model-based results, as both CTE-CH_4/Prior and Posterior ranked OH as the most important variable, while for satellite data OH was clearly less important. For satellite daily medians, there was a difference in the OH rankings between PI and RFFI, but this may be due to the high correlation between OH and soil temperature ($r = 0.87$). For TROPOMI/WFMD and CTE-CH_4/Posterior XCH_4, the partial dependencies showed a pattern that we expected based on **?**: as OH (i.e. CH_4 loss by OH) increases, the predicted XCH_4 decreases. The observed non-smooth pattern in PDPs is a result

640   of the monthly resolution of the OH data used. For the model-based results, the significant role of OH in determining XCH_4 is to some extent expected, as the similar method (Sect.2.7) for representing the OH sink is applied in the CTE-CH_4 model (Sect.2.2).

    The used method to describe the effectiveness of the OH sink is a simplification, as we assumed that large-scale OH loss, monthly zonal mean CH_4 loss values calculated for the latitude band 57–70°N, is sufficient to examine the variability of XCH_4

645   in this study. This is based on the assumption that OH loss does not vary significantly between the study areas at monthly resolution. However, this assumption does not account for the fact that OH concentrations depend on factors such as UV radiation and humidity (**??**) and reaction rates with CH_4 on air temperature, and thus exhibit shorter-term and interannual variability. This might be one reason why OH had less impact on the daily variability of satellite-based XCH_4 than in the seasonal cycle. As we focus on northern high latitudes, we are dealing with surfaces that are both spectrally and seasonally

650   variable, particularly due to snow cover, which can influence OH levels via changing UV reflectivity. For instance, **?** showed that during El Niño Southern Oscillation (ENSO) events, increased cloud cover corresponds to reduced OH concentrations, likely due to decreased near-surface UV radiation. Consequently, snow cover may impact not only methane fluxes but also the atmospheric methane sink indirectly. Studying the effectiveness of the OH sink in more detail would require more accurate OH estimates or the use of new proxies that can capture small-scale spatiotemporal variability. Given that the lifetime of OH is

655   extremely short (typically around one second), and that it is highly sensitive to perturbations in both its sources and sinks (**?**), it is challenging to measure OH directly or to model its spatial variability reliably. Until now, atmospheric methyl chloroform concentrations have often been used as a proxy for OH, however, this approach is becoming increasingly difficult as methyl chloroform levels decline (**?**).

Role of snow conditions and frozen ground

660   Snow and frost require similar conditions, specifically temperatures below zero degrees Celsius. Moreover, they are closely interconnected: snow acts as an insulating layer, influencing soil freezing and thawing. For methane emissions, snow plays an important role as it slows down methane from entering the atmosphere from the soil. Snow also contributes to soil thawing, as water from melted snow thaws the soil from above and increases the soil water volume. Studies that have carried out measurements outside the growing season have mainly focused on quantifying fluxes during the cold season and comparing

665   them to annual emissions. However, only few studies have directly studied the relationship between snow and methane fluxes, partly due to the difficulty in accessing in situ observation sites during the winter months. The cold season emissions can cover

a major part of the annual emissions, despite snow and soil frost (e.g, **??**). The emissions during the cold season are relatively stable, with a monthly distribution accounting 4–8% of the annual emissions (**?**). However, since the cold season lasts in some parts of high latitudes from early October to early May, a significant amount of emissions is accumulated over this time period and therefore the cold season emissions are important to the annual methane budget in these areas. As mentioned in Sect. 2.5, the quality of SMOS F/T product data near Russia is affected by RFI interference. However, it was observed that in our case, the interference significantly impacted the data quality only for the year 2023. Our earlier results, which did not yet include data from 2023, were consistent with the current findings. This consistency suggests that the interference has not impacted our results, which is logical given the relatively low importance of soil freezing (Fig. 4).

From the studies that have been directly investigating the connections between snow and methane, **?** found that the springtime increase in CH_4 flux was strongly correlated with the ~~date~~ timing of snowmelt. Additionally, **?** reported that earlier snowmelt and higher early summer temperatures in June has increased the early summer CH_4 fluxes in Siberian Tundra. Both **?** and **?** showed a significant rise in methane emissions over a wetland following the spring thaw, and then strong monthly emissions that lasted over the thaw season. They both defined the seasons based on temperatures, either air or soil.

Our results show that for ~~the~~ seasonal cycle, especially for the satellite-based XCH_4 ~~seasonal cycle~~, snow is a more important determining factor than for ~~the~~ XCH_4 daily medians; the amount ~~of snow determines~~ and coverage of snow help determine the phase of the XCH_4 seasonal cycle together with ~~soil moisture. However,~~ OH. For the TROPOMI/WFMD seasonal cycle of XCH_4, the partial dependence of SWE and snow cover (Figs. 5(b) and (c)) behaves as expected based on **?** and **?**: when the snow is melting or close to melting, XCH_4 increases. This pattern is visible in the seasonal cycle PDPs, whereas the curves for daily medians are flatter (Figs. 6(b) and (c)). For CTE-CH$_4$/Posterior, the snow-related partial dependence curves are nearly flat, which is as expected, since OH was clearly more important for the seasonal cycle than other environmental variables. For CTE-CH$_4$/Prior, however, the snow-related environmental variables do not behave as expected: for daily values the curves are nearly flat, but for the seasonal cycle, they show an increase in XCH_4 with increasing snow, which would imply higher methane concentrations in the presence of snow than without it. This possibly indicates inaccuracy of the LPX-Bern DYPTOP process-based model in estimating CH4 fluxes under snow conditions.

? and **?** examined the effects of snow on small, well-defined land cover types, whereas in our study, the SWE data resolution is 5 km, approximately the same as the TROPOMI pixel size. Despite this relatively ~~small grid size~~ fine resolution, it still encompasses ~~various land types with differing melting timings. Additionally~~ a mixture of land cover types with varying snowmelt timings. In addition, when averaging across the entire case study area, further variability arises due to the diverse land cover types present. As ~~shown in Sect. 3.1 in~~ listed in Table1, none of the areas had a total wetland fraction exceeding 50%, indicating that more than half of the area consists of non-wetland types. ~~In Section 4.2, we further address this uncertainty by calculating case study area specific uncertainties~~

For the model results, the significance of snow in the CTE-CH$_4$/Prior seasonal cycle of XCH_4 is somewhat surprising, as the prior fluxes are monthly and do not account for the exact annual timing of snowmelt or detailed snow cover information. Moreover, since the partial dependence behavior of snow-related variables is also not as expected, it is possible that other processes or correlations are confounded with snow in the CTE-CH$_4$/Prior results. The comparison between satellite and

model-based results suggests that the agreement in variable importance could be improved if the calculation of prior fluxes incorporated more detailed, year-specific information on snow cover and melt timing, as snow and its melting appears to play a clearly more important role in the seasonal cycle of XCH$_4$ based on satellite observations.

Role of air and soil temperature and soil moisture

Based on flux studies, it can be stated that during the growing season, there is a positive correlation between methane flux and soil temperature (e.g., **???**). This relationship is linked to microbiological activity, which is enhanced by higher soil temperatures, leading to increased methane emissions from wetlands. **?** showed that when the soil temperature is below zero, CH$_4$ emissions are small, but as the soil temperature increases toward zero and above, methane emissions begin to rise, with the highest emissions occurring during July and August. Similarly, **?** showed that emissions peak during July and August and follow the soil temperature.

According to both PI and RFFI scores, air temperature is the most important factor influencing the detrended satellite-based XCH$_4$ daily medians, although the uncertainty range for PI is relatively high. Nevertheless, air temperature remains clearly the most important variable within this range. The partial dependence plot (Fig. 6(e)) shows that when air temperature approaches two degrees, the predicted XCH$_4$ starts to increase sharply, which is theoretically in line with **?** and **?**, although in our case the variable is air temperature, not directly the soil temperature. When interpreting PDPs, it must be noted that strongly correlated variables may lead to shared attribution in the PDPs, and the correlation between air temperature and soil temperature was high ($r = 0.93$). Nonetheless, soil temperature (Fig. 6(f)) exhibits a similar trend, though clearly weaker, i.e. as temperature increases, the predicted XCH$_4$ also increases. This is consistent with the hypothesis that rising temperatures enhance methane emissions, which should in turn be reflected as an increase in total-column methane. In addition, the importance of air temperature may also reflect the influence of dynamical weather events on the daily variability of XCH$_4$. However, as the explanatory power of the RF model for TROPOMI/WFMD daily medians was relatively low ($R^2 = 0.32$), we cannot conclude that daily variability in XCH$_4$ is driven by temperature alone, since only approximately one third of the variability can be explained by the model.

The CTE-CH$_4$/Prior and CTE-CH$_4$/Posterior results mainly show a weak dependence on temperature. For the seasonal cycle, CTE-CH$_4$/Prior displays a slight increase at the highest air temperatures, while for soil temperature, both versions show a decreasing trend, which is opposite to that observed in the satellite data and expected based on in situ studies. For daily values, both model versions show a slightly increasing trend with air temperature, but a decreasing trend with soil temperature. Taken together, the importance scores and partial dependence plots suggest that the modelled XCH$_4$ responds less strongly to temperature variations compared to the satellite-based results, and does not reflect short-term fluctuations in temperature between days. This is at least partly expected, as day-to-day variability is considerably lower in the model than in the satellite data (e.g., Figs. 2(b) and (d)).

The effect of soil moisture on methane emissions is ~~a complexprocess~~complex, and the ~~results are~~process is significantly influenced by factors such as wetland type or the time period (month, season, year) being studied. For example, **?** compared methane emissions from a drained area to a ~~more moist~~moister control area at moist tussock tundra that is located on Siberian

permafrost area. They showed that the annual amount of methane emissions is correlated with ~~drainage~~soil moisture; in the drained area, annual methane emissions were lower than in the ~~moist~~ moister control areas. On the other hand, **?** studied emissions from the Alaskan tundra and showed that, at the driest sites, cold-season emissions dominated the annual emissions. ~~Based on our importance analysis,~~ Our results do not indicate a systematic impact of soil moisture on XCH_4 variability as the

740 ranking of soil water volume ~~, which describes soil moisture, is strongly linked to the seasonal variability of XCH_4. However, its influence in the shorter-term variability is more complex, making it difficult to capture using simple statistical measures, such as the Pearson correlation coefficient. This complexity~~ varies between satellite-based and model-based data and seasonal cycle and daily values (Table A2). In addition, the importance scores of soil moisture are generally low (table A1).

The lack of systematic response may arise from relatively strong day-to-day variability in soil moisture during the summer, as

745 well as significant local variations, such as differences in soil types ~~(e.g., **?** and their comparison between two adjacent areas).~~ (e.g., **?**, and their comparison between two adjacent areas). **?** studied how process-based ecosystem models responded to air temperature and precipitation in Fennoscandia. They found that models with a more pronounced peatland component were more temperature-driven, whereas models with a more pronounced wet mineral soil component were more precipitation-driven. The CTE-CH$_4$ posterior wetland emissions, based on fluxes from two models with contrasting response patterns, depended

750 on both air temperature and precipitation. In addition, **?** found that when large-scale methane emissions were studied, the process-model based methane emissions increased when the snow melted and the soil thawed, and at the same time, the air temperature rose above zero degrees Celsius. They also observed a peak in methane fluxes caused by inundation component, potentially caused by melted snow. Since the environmental variables used in this study are relatively sparse in spatial grid resolution and are then averaged over larger areas, there are inevitably many different land cover and wetland types within each

755 grid cell and within the case study area. ~~Furthermore, the soil water volume in Layer 1 represents soil moisture in the topsoil, and it is possible that methane emissions during the summer are more influenced by water table depth, which changes more slowly than topsoil moisture. The Layer 1 was chosen because it represents the soil properties in the 0–7 cm layer, while Layer 2 represents the 7–28 cm depth, and we wanted to select the layer closest to the surface. Both layers were not chosen because their correlation was really close to one, which would have made the interpretation of PI and RFFI importance values more~~

760 ~~difficult. In permafrost areas, the active permafrost layer depth might also have an effect.~~ To study the effect of soil moisture on XCH_4 at a more detailed level, it would likely be necessary to consider different soil types individually, permafrost areas, and the relationship between soil moisture and individual XCH_4 satellite observations. ~~Additionally, spatially representative data on water table depth would be valuable, as methane emissions continue when the water table drops below the 7 cm depth observed in topsoil moisture, but they cease in deeply drained soils and turn into a methane sink. In permafrost regions, it~~

765 ~~would also be valuable to study the seasonal development of active layer depth, as it determines the thickness of the soil layer emitting methane.~~ We tested the analysis using satellite-based soil moisture data ~~(**?**), but the main issue was that~~ (**?**) but it is not daily data, and there were significant data gaps during springtime. This prevented a comprehensive ~~analysis with that data~~ satellite-based analysis and was the reason to use ERA5 soil water volume instead.

~~Based on flux studies, it can be stated that during the growing season, there is a positive correlation between methane~~
~~flux and soil temperature (e.g., **???**). This relationship is linked to microbiological activity, which is enhanced by higher soil~~
~~temperatures, leading to increased methane emissions from wetlands. According to both~~

Synthesis of satellite and model results

The similarities and discrepancies between the PI and RFFI scores ~~, soil temperature is the most important factor influencing~~ ~~the detrended~~ and the PDPs suggest that, for the TROPOMI/WFMD XCH_4 ~~daily medians, although for PI,~~ seasonal cycle, the RF model performs relatively consistently. OH and SWE emerge as the main drivers of the seasonal cycle, and their influence aligns with physical expectations based on in situ observations. The robustness of the results is further supported by the high explanatory power of the model, as indicated by the coefficient of determination for the seasonal cycle ($R^2 = 0.73$), showing that the ~~uncertainty range is high. Nevertheless, soil temperature remains the most important within this range. **?** showed that~~ ~~when the soil temperature is below zero, CH~~model captures most of the seasonal variability. However, for the satellite-based short-term XCH_4 ~~emissions are small, but as the soil temperature increases toward zero and above, methane emissions begin~~ ~~to rise, with the highest emissions occurring during July and August. Similarly, **?** showed that emissions peak during July~~ ~~and August and follow the temperature. We examined the correlation between soil temperature and~~ variability, the ~~detrended~~ ~~XCH~~RF model is less stable, indicating that the mechanisms explaining daily variability are more complex and that short-term environmental variability has little systematic impact in the total column, which is reasonable. This is reflected in the lower coefficient of determination ($R^2 = 0.32$). Nonetheless, our results on the effect and importance of temperature are consistent with in situ studies that demonstrate the role of temperature in driving methane variability.

We expected differences between the satellite and model-based results, as it has been shown that the CTE-CH$_4$ ~~daily~~ ~~median for each month separately and found that, during the period from May to August, the correlation between the daily~~ ~~mean soil temperature and the detrended~~ model, and inversion models in general, estimate global total emissions well, while regional estimates are strongly dependent on the prior emission datasets used (e.g., **?**). In our analysis, we used surface observation-based posterior results, meaning that the posterior fluxes are optimized to match surface methane concentrations. However, part of the XCH_4 ~~daily median was moderate, with Pearson correlation coefficients of 0.34, 0.39, 0.48, and 0.32,~~ ~~respectively. During the other months, the correlation was not larger than 0.3, but in April and October, it ranged between~~ ~~0.2 and 0.3. Although the Pearson correlation coefficients are relatively low, our results regarding the significance of soil~~ ~~temperature are consistent with previous research, which shows that temperature affects methane emissions. We observe this~~ ~~in the~~ variability originates in the upper atmosphere. For example, the OH sink is not specifically located near the surface (**?**). Also, in the optimization, there was a difference between 2018–2021 and 2022: for 2022, no surface observations were available from Russia, which covers a large part of the high-latitude region.

Generally, we found that the environmental variables had a stronger and more consistent effect on TROPOMI/WFMD and CTE-CH$_4$/Posterior than on CTE-CH$_4$/Prior. Also, the mechanisms through which environmental variables influenced the total-column concentrations were better explained and more coherent for TROPOMI/WFMD and CTE-CH$_4$/Posterior than for the Prior. For example, increasing OH sink led to a decreasing response in total-column methane for both TROPOMI/WFMD

and CTE-CH$_4$/Posterior, whereas for CTE-CH$_4$/Prior, the response was irregular and even increasing. This decreasing response is expected, as the OH sink is the main removal process of methane in the atmosphere. The effect of snow was fairly weak in CTE-CH$_4$/Posterior, while for TROPOMI/WFMD, an decreasing amount of snow corresponded to the increasing phase of the XCH$_4$ seasonal cycle, i.e. when snow melts methane increases. In contrast, for CTE-CH$_4$/Prior, the seasonal cycle increased with increasing snow amount and coverage, which is not consistent with expectations based on in situ results. It should be noted that these results apply only to spring, as our time series was limited by the winter gap in satellite observations. If winter periods had been included, they would have required a separate analysis, although it remains unclear how XCH$_4$ ~~data, and~~ behaves during winter in high Northern latitudes. During this period, wetland emissions are minimal, and the OH sink is also weak due to the absence or low level of sunlight. Therefore, no conclusions can be drawn regarding winter conditions, and the results presented here apply exclusively to the ~~low correlations may be attributed to the fact that methane emissions may respond with a delay to changes in temperature. The random forest model, which can incorporate time lags, likely explains why, despite the low correlations, soil temperature still shows significant importance in the model.~~

~~OH became a significant factor based on the RFFI importance score for~~ spring–summer period.

The time series of CTE-CH$_4$/Prior, CTE-CH$_4$/Posterior, and TROPOMI/WFMD showed that the background level of total-column methane concentrations differs between datasets (e.g., Figs. 2(a) and (c)), with the model consistently overestimating XCH$_4$ ~~daily medians, likely due to its high correlation with soil temperature (r = 0.87). As noted in Sect. 3.5, highly correlated variables may share the assigned importance in the random forest model when using RFFI. However, PI importance score is not as sensitive as RFFI for this sharing effect, and in the PI scores, OH ranks as the third most important factor, though it has significantly less influence compared to soil temperature or SWE (Figs. 4 and ??).~~ across regions and years. This feature has been noted previously by **?**, and potential causes include vertical transport (stratosphere–troposphere exchange), atmospheric chemistry, tropopause height estimation, and model resolution in both horizontal and vertical directions (**??**). These may also contribute to the differences in environmental variable importance for the model-based seasonal cycles: for CTE-CH$_4$/Prior, snow amount was found to be the most important variable and OH sink the second, whereas for CTE-CH$_4$/Posterior, the OH sink was clearly dominant, with other environmental variables being much less important and having only small differences between them. It seems that when optimizing the posterior fluxes, the model tries to produce the seasonality of the sinks rather than the sources. In addition, ~~it should be noted that we used monthly zonal mean CH$_4$ loss values from TM5, calculated for the latitude zone 57°N~~ since we used a surface-data based inversion, the model do not necessary aims to match the total column concentrations, which have different phases in seasonal cycles (e.g., **?**).

The transport model was run on a relatively coarse spatial resolution of $6° \times 4°$, which corresponds to roughly 200 to 350 km in the west–~~70°N (see Sect. 2.7). The method used is a simplification; we assumed that the large-scale OH loss is sufficient to examine the variability of XCH$_4$ in this study. This is based on the assumption that OH loss would not vary significantly spatially between the study areas at a monthly resolution. However, this assumption does not take into account that OH concentrations depend on factors such as the amount of UV radiation and humidity (??), and therefore, it has also shorter-term and interannual variability. As we concentrate on the Northern high latitudes, we are dealing with spectrally and temporally variable surfaces, particularly seasonal snow cover, which can influence OH levels due to varying UV reflection from the~~

surface. For instance, **?** presented that during El Niño east direction and nearly 450 km in the south–Southern Oscillation (ENSO) events, increased cloud cover corresponds to lower OH concentrations , likely due to reduced UV radiation near the surface. Consequently, snow cover may impact not only methane fluxes but also the atmospheric methane sink indirectly. A more detailed and deeper evaluation the effectiveness of north direction. Compared to TROPOMI pixel size, the OH sink would require more accurate OH estimation or the use of new proxies to demonstrate small-scale variations in OH concentrations. Given that the lifetime of OH is very short, typically approximately one second, and it is highly sensitive to disturbances in both its sources and sinks (**?**) it is challenging to measure OH concentrations or reliably model its concentration spatial variability in the atmosphere. Until now, atmospheric measurements of methyl chloroform have often been used as a proxy for OH concentration; however, this approach is becoming increasingly difficult as methyl chloroform concentrations decline (**?**).

5.2 Seasonal timing of XCH$_4$ minima and maxima in relation to snow

model grid cell area is over 2,000 times larger, and each grid cell contains a wide range of land cover types and environmental conditions. The same applies to our case study areas, which also exhibit considerable variation in land cover and environmental conditions. For the satellite data, we used the daily median to reduce the influence of within-area variability, so that each daily median represents a central estimate across the region. In addition, as discussed earlier, day-to-day variability is significantly higher in the satellite observations than in the model, which is expected, since the modelled daily concentrations are based on weekly posterior fluxes and monthly prior fluxes, making it challenging to capture finer temporal dynamics.

Scatter plots show (a) onset of snowmelt (y-axis) versus the day of the year when the XCH$_4$ seasonal cycle reaches its minimum (x-axis), and (b) the end of snowmelt (y-axis) versus the day of the local maxima in XCH$_4$ (x-axis). Both figures also display the one-to-one line in gray dots, a linear fit as a black dotted line, and an Orthogonal Distance Regression (ODR) fit as a black dashed line. The ODR fit accounts for uncertainties in both directions, with all uncertainties calculated based on the data. Generally, our satellite-based findings support the results of **?**, who used multiple chemical transport model simulations and found that the magnitude, latitudinal distribution, and seasonality of wetland emissions are critical for the methane seasonal cycle in the Northern Hemisphere, as they determine the timing and magnitude of the summer increase. Our results highlight the importance of OH and further specify this relationship between the seasonal cycle and wetland emissions by demonstrating that environmental variables directly linked to wetland emissions, such as temperature and SWE, including water from snow melt, are key factors for methane production in high-latitude wetlands, either directly or indirectly, by influencing the soil water cycle and soil temperature.

5.2 Seasonal timing of XCH$_4$ minima and maxima in relation to snow

Snow influences wetland methane emissions in multiple ways, for instance, it acts as an insulating layer for the soil, affecting soil temperatures and freezing processes, thereby directly impacting methane production in the soil. Snow also slows down the methane emissions from entering to the atmosphere from the soil. In spring, as snow melts, a pulse of methane emissions is often observed, resulting from methane that accumulated beneath the snow and ice during winter being released after the snowmelt and soil melt (**?**). Additionally, soil moisture is closely linked to snowmelt in spring; Figs. C3, 3, and C4 show that

in the Siberian case study areas, soil water volume typically increases sharply to a distinct peak during the period between the onset and the end of snowmelt. This increase in soil water volume is linked directly to melting snow. In Northern and Southern Finland, this pattern is less distinct, though similar features can still be observed to some extent (Figs.C1 and C2).

Our results in Sect. 4.1 showed that the seasonal cycle of XCH_4 is also influenced by snow. To further investigate the temporal connection between snow and the seasonal cycle of XCH_4, we focused on spring, particularly in the minimum XCH_4 in early spring and the local maxima in late spring or early summer, along snowmelt. The focus on spring was chosen because the annual maximum often coincides with time when TROPOMI observations are not possible, and the onset of snow cover frequently falls within this timeframe (Fig. D1), complicating the analysis. The impact of the winter gap on our analysis and the added value of increasing satellite observations during the winter gap in XCH_4 data are discussed in more detail at the end of this section. For the analysis, we defined the end of snowmelt based on snow cover, rather than SWE, because it is a simpler method for determination, and in SWE time series, it is observed that significant amounts of snow may still fall after SWE approaches zero, for example, in Fig. 3(c) in the spring of 2020. When determining the end of snowmelt based on snow cover, these situations were more precisely defined. The onset of snowmelt, however, must be defined through the start of SWE reduction, as SWE begins to decrease much earlier than snow cover (Fig. D1). Threshold-based methods for defining the onset and end of snowmelt are described in Sect. 3.4.

The seasonal cycle of XCH_4 reaches its minimum in early spring and its maximum during the autumn or winter. Toward the end of spring, in certain years, local minima and maxima in the XCH_4 cycle are observed across specific case study areas, coinciding with the timing of snowmelt (Fig. D1). Figure 7 shows (a) the day of minimum XCH_4 relative to onset of snowmelt, and (b) the day of local maxima in XCH_4 compared to the end of snowmelt. Both plots include a linear fit, represented by a dotted line, and an Orthogonal Distance Regression (ODR) fit, indicated by a dashed line. The ODR approach accounts for uncertainties in both the x and y directions. Both figures also display the Pearson correlation coefficient r and the coefficient of determination r^2. Uncertainties related to the timing of snowmelt and the phase of the XCH_4 seasonal cycle are calculated as presented in detail in Sections 3.3 and 3.4.

Based on Fig. 7(a), the onset of snowmelt correlates with the day of the XCH_4 minimum, within uncertainties. However, in the Southern Finland case study area, a few outliers are observed, specifically in the springs of 2020 and 2021 (Fig. 7(a)), when SWE showed a gradual decline without a clear, rapid drop, and substantial variability was present within the region (Fig. D1). The correlation between the onset of snowmelt and the day of minimum XCH_4 is moderate, with a correlation coefficient of 0.54. When the two Southern Finland outlier years are excluded, however, the correlation strengthens substantially, with a coefficient of 0.74. The correlation between the day of the local maxima in XCH_4 and the end of snowmelt is moderately strong, with a Pearson correlation coefficient of 0.66. Both the linear and ODR fits are close to the 1:1 line, suggesting that the local maxima in XCH_4 generally occur around the time when the snow cover has fully melted.

In situ and modeling studies have mainly focused on the effect of soil freeze and thaw on methane emissions rather than on the impact of snow (e.g., **??**). Based on previous studies, we were not able to draw clear conclusions regarding whether the coinciding of onset of snowmelt and the day of minimum XCH_4 is a result of each other. This uncertainty originates from

905 limited knowledge about the amount of methane released during the early stages of snowmelt, when snow cover persists and the soil may still be frozen. ~~The~~

The possible correlation between the day of local maxima in XCH$_4$ and the end of snowmelt ~~is likely~~ may be related to the known connections between snow and methane, as ~~presented~~ discussed in Sect. ~~4.1, where we referenced, for~~ 5.1. For example, ~~?, who~~ showed a strong correlation between the springtime increase in CH$_4$ and the ~~date of snowmelt. In addition,~~ timing of

910 snowmelt, and ? observed emission pulse during intense melting.

~~Although our importance analysis(Sect. 4.1) did not show that the loss of CH$_4$ due to the OH sink significantly affects the seasonal variability of XCH$_4$, Fig. D1 shows that the day of the local~~ However, in our analysis, the correlation between the day of local maxima in XCH$_4$ ~~minimum often coincides with or occurs in July, when the CH$_4$ loss by OH is at its maximum (e.g., Fig. 3). When considering methane concentrations in high-latitude northern wetland areas, wetland methane emissions~~

915 ~~are most intense during the summer and growing season, while the the effect of OH sink in reducing methane concentrations is also at its highest. These effects essentially counteract each other. Although we were not able to directly observe or demonstrate this opposing influence from our results, it should still be considered when interpreting the findings. This also highlights the importance of incorporating more accurate OH fields or utilizing new proxies for OH, as discussed in Sect. 4.1, to enable a more precise analysis.~~ and the end of snowmelt was not statistically significant, likely due to the limited number of observation

920 points. Further analysis of this potential relationship would require a larger dataset to either prove or disprove this hypothesis.

? showed that the hourly mean emissions during spring thaw are lower than those during autumn freeze at high-latitude tundra sites. Additionally, the mean duration of spring thaw is typically less than a month (?), whereas autumn freeze lasts nearly two months ~~. Since the effects of spring snowmelt are evident in~~ (?). Since our analysis suggests that spring snowmelt may influence the seasonal cycle of XCH$_4$~~based on our analysis~~, it is reasonable to expect that the impact of autumn snow

925 onset or soil freeze could also be detectable if we had the necessary observations. Based on Fig. D1, the winter gap begins between late October and mid-November and ends between mid-February and late March, depending on the year and case study area. The winter gap occurs because Northern regions experience very large solar zenith angles (SZA) during this period, with a period of no sunlight at all in areas above the Arctic Circle. The interannual variation in the winter gap duration is mostly driven by cloud cover and other meteorological conditions. These winter challenges are similar to what is expected for the upcoming

930 missions, e.g Copernicu's Sentinel-5, CO2M, and GOSAT-GW. Consequently, reducing the winter gap and analyzing the effect of autumn freeze on XCH$_4$ remains a particularly challenging task. However, for instance, methane observations in the thermal-infrared range could be used to address this, especially if combined with data from current shortwave infrared observations, or active observations (e.g., upcoming MERLIN mission).

935 Studies directly utilizing GHG satellite observations provide valuable information to complement atmospheric inversion results and offer ~~new~~ insights that can ~~ultimately~~ help reduce uncertainties in the global methane budget ~~while improving~~ and improve our understanding of ~~the~~ increasing and variable ~~trends in methane concentrations. To deepen our knowledge of~~

the factors directly influencing observed methane concentrations, this study investigated the dominant environmental variables that explain the seasonal variability of column-averaged methane . trends. To better understand the factors influencing observed total-column methane, we studied the links between environmental variables and satellite-based XCH_4, and assessed the impact of different drivers for the variability in different time scales. These include the fitted seasonal cycle, which captures the seasonal changes and their interannual variability but cannot detect short-term variations or extremes, and day-to-day variability, which is more sensitive to small-scale atmospheric changes and can exhibit larger fluctuations than the seasonal cycle. In addition, we performed a similar analysis for model-based prior and posterior (optimised with surface methane concentrations) total-column concentrations to examine how environmental drivers are captured in the model output and how they compare with satellite-based results.

Based on previous in situ measurement based studies , we focus our analysis studies for wetland methane emissions, we choose to focus on snow, soil freeze and thaw, temperature, soil moisture, and the impact of the OH sink. Based on our results, we further study the connections between the snowmelt We further examine the connection between snowmelt timing and the phase of the seasonal cycle of XCH_4 . Our seasonal cycle. The analysis covers the period from 2018 to 2023 and focuses on includes five case study areas , including over Northern high latitude wetlands, two in Finland and three in Siberia. The satellite-based XCH_4 data used in this study (TROPOMI WFMD v1.8) shows good agreement with reference datasets across all seasons (**?**), supporting its reliability in capturing both seasonal and daily variability throughout the study period. The analysis was performed using the random forest regression method, applying PI and RFFI importance scores, which describe the influence of each variable on the observed methane concentrations variability. In addition, we used partial dependence plots to examine the relationship between individual variables and the predicted XCH_4, allowing us to explore how the variables behave and whether their effects are physically interpretable as expected.

Our results suggest show that the main drivers of the seasonal variability of in satellite-based column-averaged methane (XCH₄) over Northern high over high Northern latitude wetland areas are soil moisture the OH sink and snow, especially particularly snow water equivalent. During the period when the soil is thawed, the The main driver of day-to-day variability in satellite-based XCH_4 is soil air temperature. Other environmental variables considered included in this study showed some effect on influence on both the seasonal cycle and day-to-day daily variability of XCH_4, but their influence was less significant compared to snow and soil moisture effects were less pronounced compared to OH, snow, and temperature. These findings are based on satellite data analysis and cover much larger areas than in situ measurements but still, the results align with and are further validated by previous in situ and model studies. studies. Our results showed partial agreement in the environmental drivers influencing satellite-based and model-based XCH_4. The posterior results after in situ data assimilation were better aligned with the satellite-based results than the prior, showing that there is already some consistency between the modeled and observed total-column methane dynamics. Although we applied multiple approaches to evaluate the robustness of the RF model and the resulting feature importance rankings, we acknowledge that strong correlations between environmental variables remain a potential source of bias in the results. In addition, for day-to-day variability, the random forest model was able to explain only about one third of the total variation, suggesting that the environmental variables included in the analysis do not fully account for the short-term variability, which can be expected due to the significant impact of transport.

Our results emphasize the need for more regionally focused model configurations and for prior emissions with higher spatial and temporal resolution, including daily snow cover and snowmelt timing, to better reproduce the satellite-based concentrations and seasonal cycles, and better capture the environmental processes behind methane emissions. However, addressing this would require significant computational resources and improved in situ and ground-based understanding of how methane fluxes and concentrations evolve during snowmelt. Nevertheless, the model results were able to capture some of the same mechanisms and patterns as the satellite-based data, which is a notable achievement given the substantial differences in spatial and temporal resolution. Moreover, our findings showed that the surface-based inversion posterior results were more aligned with the satellite observations than the prior. This indicates that while there is clear room for improvement in model priors and configurations, particularly in the stratosphere, there is already some consistency between the modeled and observed total-column methane dynamics. In addition, as the role of OH is found important in determining the seasonal cycle of XCH_4, it would be valuable to have a more spatially and temporally variable product to describe its effect, as the method used was simplified both temporally and spatially.

To investigate the connection between snow dynamics and the XCH_4 seasonal cycle, we conducted a time series analysis. The results indicate that the phase of the seasonal cycle is associated with snowmelt timing: XCH_4 minima typically occur near the onset of snowmelt, while local maxima tend to coincide with its end. The correlation between the minima and snowmelt onset was statistically significant, whereas the association with snowmelt end was not, likely due to a smaller number of observations. Although snowmelt alone cannot account for the observed increase in XCH_4, the timing suggests a potential link, possibly related to the insulating properties of snow and the subsequent release of water into the soil. These relationships should be further investigated with larger datasets or in-situ measurements to improve confidence in the results.

Our analysis focused exclusively on spring and summer, as the onset of snowfall in autumn coincides with the winter gap in satellite methane observations, making it difficult to reliably study the XCH_4 seasonal cycle during a period with no data. Acquiring observations from autumn and winter would be essential to determine whether the onset of freezing and snow cover can be detected from the XCH_4 seasonal signal. Accurately quantifying the amplitude of the seasonal cycle is also important, as it is directly related to the magnitude of CH_4 fluxes. In addition to emission-related dynamics, understanding the role of the OH sink, especially in relation to day-to-day variability and the influence of the summer maximum, could be improved by exploring new proxies that describe the effectiveness of the OH sink.

Overall, our findings suggest that satellite-based XCH$_4$ observations are suitable for studying the seasonal variability of methane on a large scale. We also find substantial local differences in both seasonal cycles and day-to-day variability. In addition, the model comparison shows interesting differences between the satellite and model results that call for further investigation. This study demonstrates how the combination of different satellite , and model , and model datasets can be used to investigate the underlying physical processes driving environmental phenomena.

. The WFMD XCH$_4$ data is available at https://www.iup.uni-bremen.de/carbon_ghg/products/tropomi_wfmd/. IMS snow cover data is available at https://noaadata.apps.nsidc.org/NOAA/G02156/. The Copernicus Global Land Monitoring Service SWE product is available at https://land.copernicus.eu/en/products/snow/snow-water-equivalent-v1-0-5km. ERA5 2 m temperature, soil temperature and soil water volume at layer 1 are available at https://cds.climate.copernicus.eu/cdsapp#!/dataset/reanalysis-era5-single-levels.

Appendix A: Importance tables

Table A1. Mean permutation importance (PI) and random forest feature importance (RFFI) scores for TROPOMI/WFMD, CTE-CH4/Prior, and CTE-CH4/Posterior, for each environmental variable in predicting the seasonal cycle and detrended daily values of XCH_4.

			OH	SWE	snow	F/T	T/L1	SM	T/2m
TROPOMI / WFMD v1.8	XCH_4 seasonal cycle	PI	0.50	0.30	0.19	0.14	0.15	0.12	0.06
		RFFI	0.19	0.18	0.11	0.12	0.15	0.13	0.13
	Detrended XCH_4 daily medians	PI	0.20	0.08	0.03	0.04	0.07	0.07	0.52
		RFFI	0.08	0.15	0.05	0.08	0.21	0.18	0.24
CTE-CH4 / Prior	XCH_4 seasonal cycle	PI	0.37	0.44	0.29	0.16	0.12	0.05	0.06
		RFFI	0.17	0.25	0.18	0.13	0.12	0.06	0.09
	Detrended XCH_4 daily values	PI	0.34	0.25	0.24	0.13	0.10	0.09	0.09
		RFFI	0.12	0.20	0.13	0.10	0.16	0.13	0.15
CTE-CH4 / Posterior	XCH_4 seasonal cycle	PI	0.62	0.08	0.06	0.06	0.12	0.08	0.05
		RFFI	0.33	0.07	0.06	0.07	0.21	0.08	0.17
	Detrended XCH_4 daily values	PI	0.42	0.10	0.07	0.06	0.11	0.10	0.09
		RFFI	0.19	0.11	0.06	0.06	0.22	0.16	0.20

Table A2. Variable importance rankings based on permutation importance (PI) and random forest feature importance (RFFI) for TROPOMI/WFMD, CTE-CH$_4$/Prior, and CTE-CH$_4$/Posterior. Rankings are shown separately for the seasonal cycle and detrended daily values of XCH$_4$, for each environmental variable. Lower rank indicates higher importance (1 = most important).

			OH	SWE	snow	F/T	T/L1	SM	T/2m
TROPOMI / WFMD v1.8	XCH$_4$ seasonal cycle	PI	1	2	3	5	4	6	7
		RFFI	1	2	7	6	3	4	5
	Detrended XCH$_4$ daily medians	PI	2	3	7	6	4	5	1
		RFFI	6	4	7	5	2	3	1
CTE-CH4 / Prior	XCH$_4$ seasonal cycle	PI	2	1	3	4	5	7	6
		RFFI	3	1	2	4	5	7	6
	Detrended XCH$_4$ daily values	PI	1	2	3	4	5	7	6
		RFFI	6	1	5	7	2	4	3
CTE-CH4 / Posterior	XCH$_4$ seasonal cycle	PI	1	3	5	6	2	4	7
		RFFI	1	5	7	6	2	4	3
	Detrended XCH$_4$ daily values	PI	1	3	6	7	2	4	5
		RFFI	3	5	7	6	1	4	2

Appendix B: XCH$_4$ time series and fitted seasonal cycles
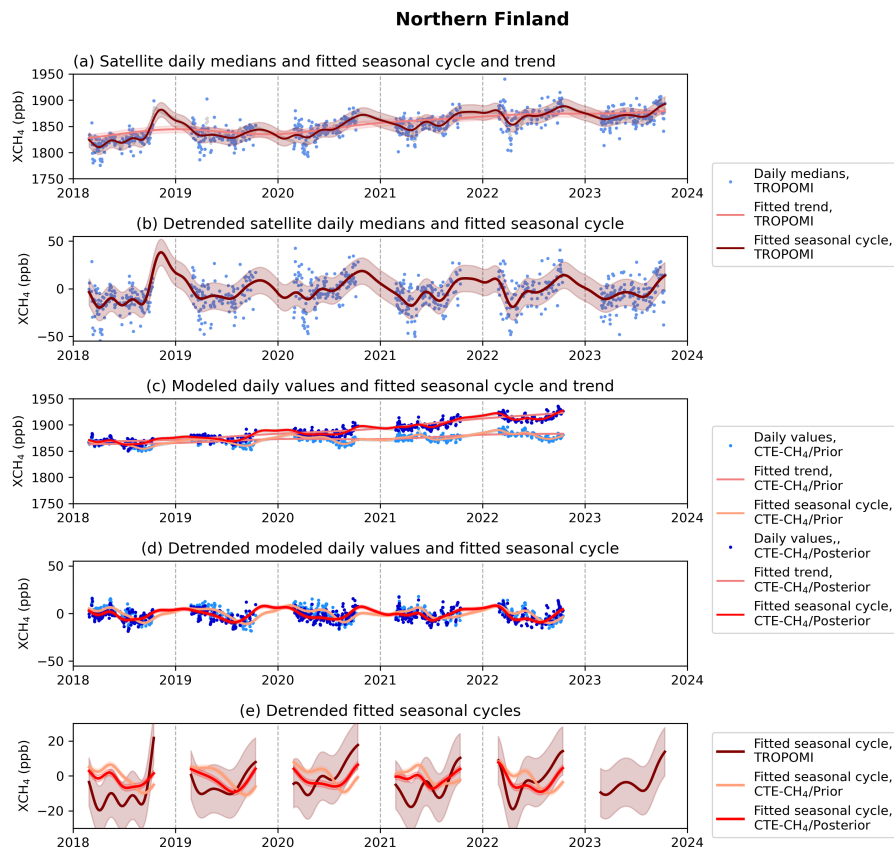
Figure B1. (a) TROPOMI WFMD daily median XCH$_4$ values (blue dots) with the fitted seasonal cycle and trend, ~~gap-filled~~ including their uncertainties (red and shaded red), for Northern Finland. (b) Same as (a), but detrended TROPOMI WFMD XCH$_4$ time series. (c) CTE-CH$_4$ prior and posterior daily XCH$_4$ values (~~grey~~ lighter and darker blue dots, respectively)~~and~~, along with the fitted seasonal cycle and trend, and their uncertainties (lighter and darker red lines, and corresponding shaded ~~red~~ areas)~~for Northern Finland~~. (~~b~~d) ~~shows the same for the~~ Same as (c), but detrended CTE-CH$_4$ time series. (e) Detrended fitted seasonal cycles and their uncertainties for TROPOMI WFMD and CTE-CH$_4$ prior and posterior XCH$_4$.
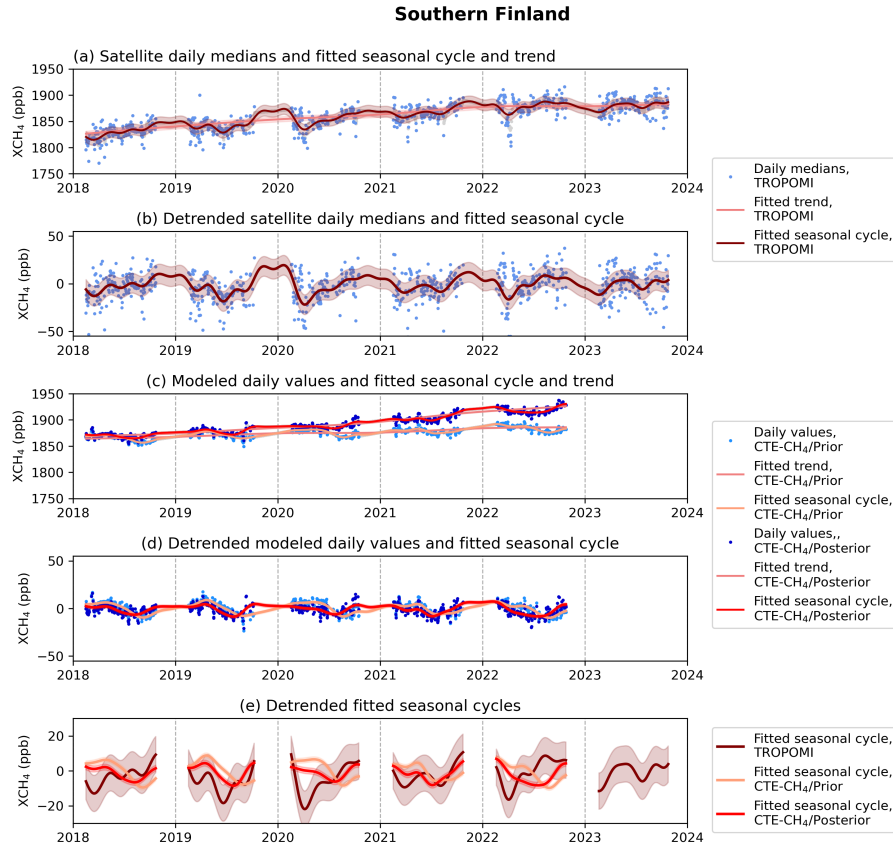
Figure B2. (a) TROPOMI WFMD daily median XCH$_4$ ~~values~~ (blue dots) with the fitted seasonal cycle and trend, ~~gap-filled~~ including their uncertainties (red and shaded red), for Southern Finland. (b) Same as (a), but detrended TROPOMI WFMD XCH$_4$ time series. (c) CTE-CH$_4$ prior and posterior daily XCH$_4$ values (~~grey~~ lighter and darker blue dots, respectively) ~~and~~, along with the fitted seasonal cycle and trend, and their uncertainties (lighter and darker red lines, and corresponding shaded ~~red~~ areas) ~~for Southern Finland~~. (~~b~~d) ~~shows the same for the~~ Same as (c), but detrended CTE-CH$_4$ time series. (e) Detrended fitted seasonal cycles and their uncertainties for TROPOMI WFMD and CTE-CH$_4$ prior and posterior XCH$_4$.
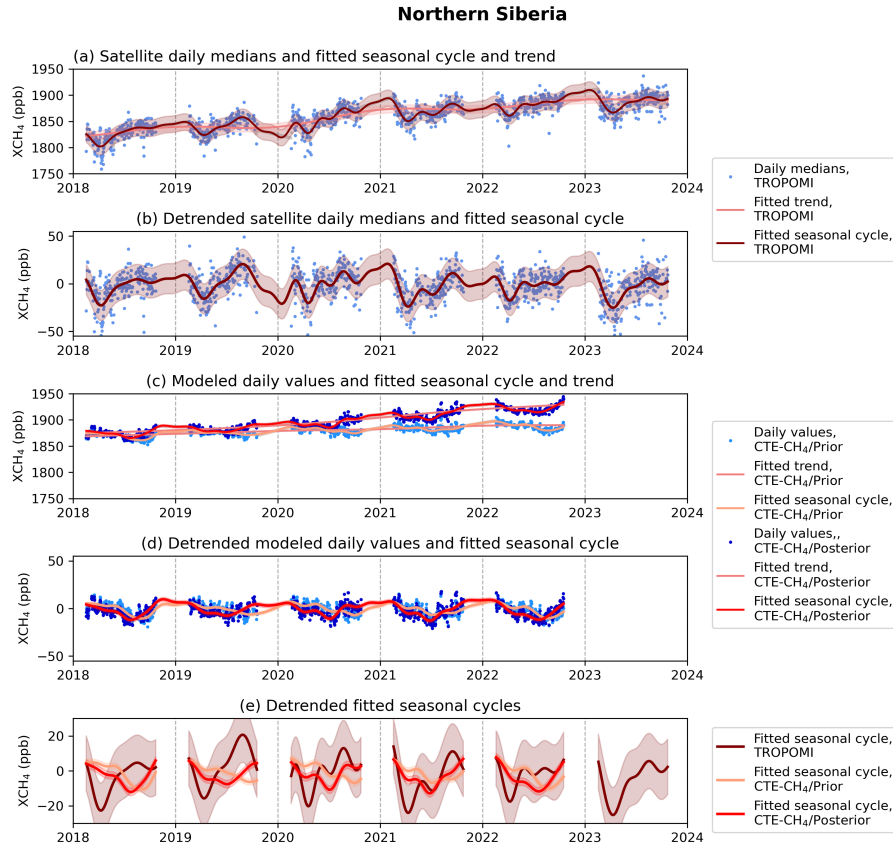
Northern Siberia

Figure B3. (a) TROPOMI WFMD daily median XCH$_4$ values (blue dots) with the fitted seasonal cycle and trend, ~~gap-filled~~ including their uncertainties (red and shaded red), for Northern Siberia. (b) Same as (a), but detrended TROPOMI WFMD XCH$_4$ time series. (c) CTE-CH$_4$ prior and posterior daily XCH$_4$ values (~~grey~~ lighter and darker blue dots, respectively)~~and~~, along with the fitted seasonal cycle and trend, and their uncertainties (lighter and darker red lines, and corresponding shaded ~~red~~areas)~~for Northern Siberia~~. (~~b~~d) ~~shows the same for the~~ Same as (c), but detrended CTE-CH$_4$ time series. (e) Detrended fitted seasonal cycles and their uncertainties for TROPOMI WFMD and CTE-CH$_4$ prior and posterior XCH$_4$.

Southern Siberia
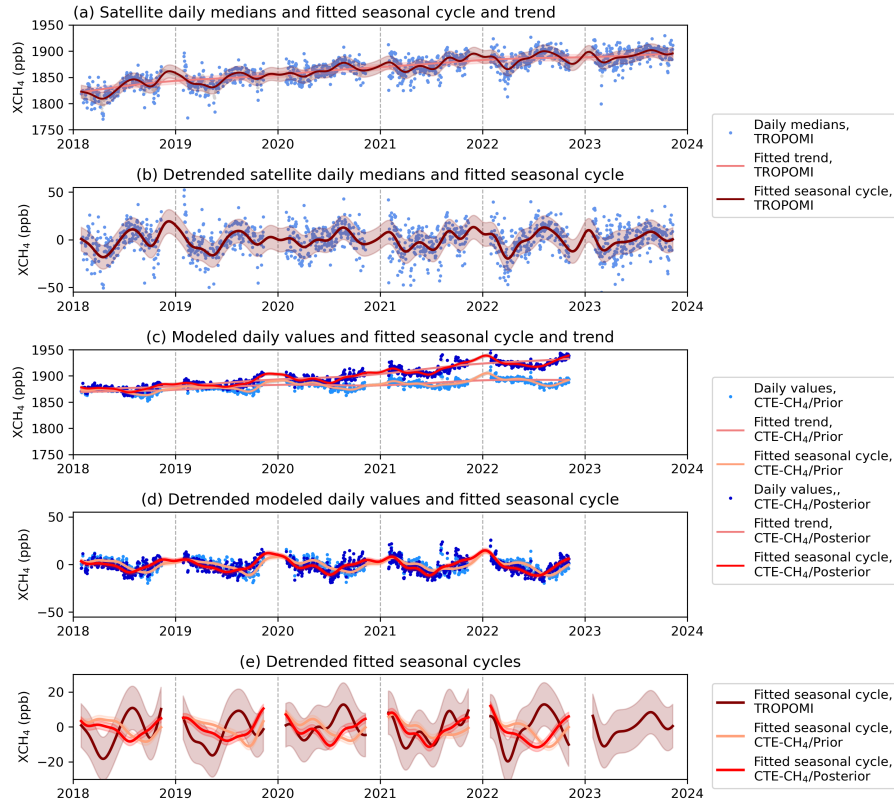
Figure B4. (a) TROPOMI WFMD daily median XCH$_4$ values (blue dots) with the fitted seasonal cycle and trend, ~~gap-filled~~ including their uncertainties (red and shaded red), for Southern Siberia. (b) Same as (a), but detrended TROPOMI WFMD XCH$_4$ time series. (c) CTE-CH$_4$ prior and posterior daily XCH$_4$ values (~~grey~~ lighter and darker blue dots, respectively)~~and~~, along with the fitted seasonal cycle and trend, and their uncertainties (lighter and darker red lines, and corresponding shaded ~~red~~areas)~~for Southern Siberia~~. (~~b~~d) ~~shows the same for the~~ Same as (c), but detrended CTE-CH$_4$ time series. (e) Detrended fitted seasonal cycles and their uncertainties for TROPOMI WFMD and CTE-CH$_4$ prior and posterior XCH$_4$.

Appendix C: Environmental time series
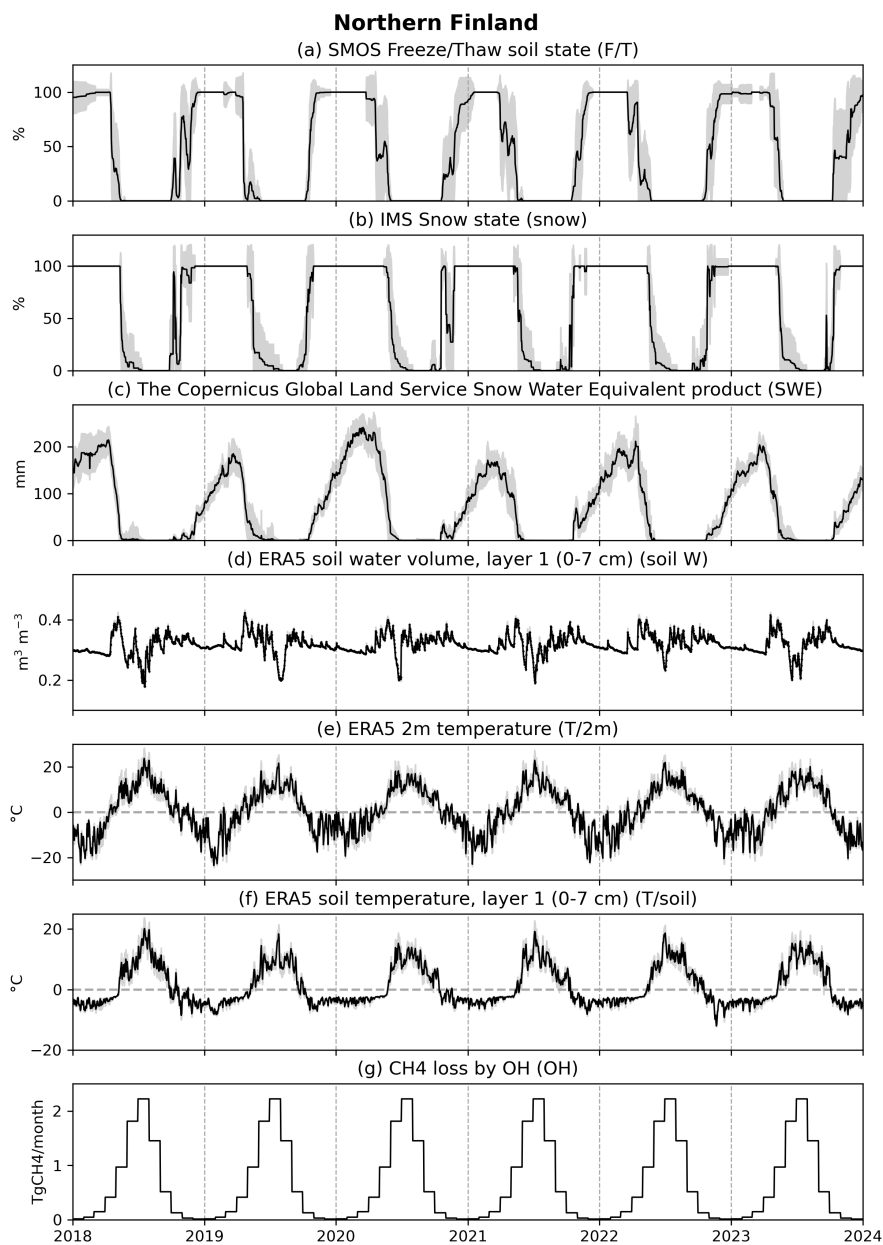
Figure C1. Black line shows the daily mean and the filled grey area the standard deviation of (a) soil freeze-thaw state, (b) snow cover state, (c) snow water equivalent, (d) layer 1 soil water volume, (e) 2 meter air temperature, (f) layer 1 soil temperature and (g) CH$_4$ loss by OH for Northern Finland.
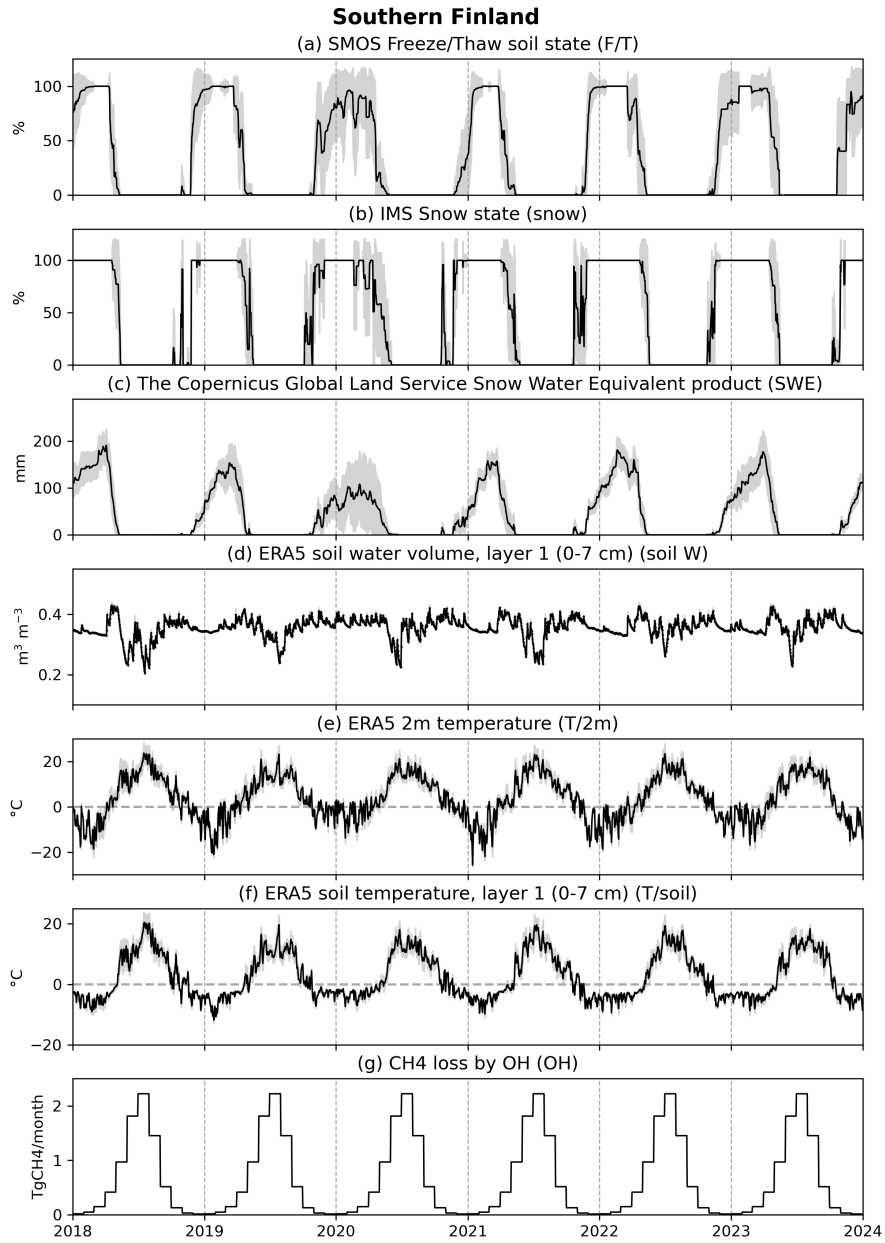
Figure C2. Black line shows the daily mean and the filled grey area the standard deviation of (a) soil freeze-thaw state, (b) snow cover state, (c) snow water equivalent, (d) layer 1 soil water volume, (e) 2 meter air temperature, (f) layer 1 soil temperature and (g) CH_4 loss by OH for Southern Finland.
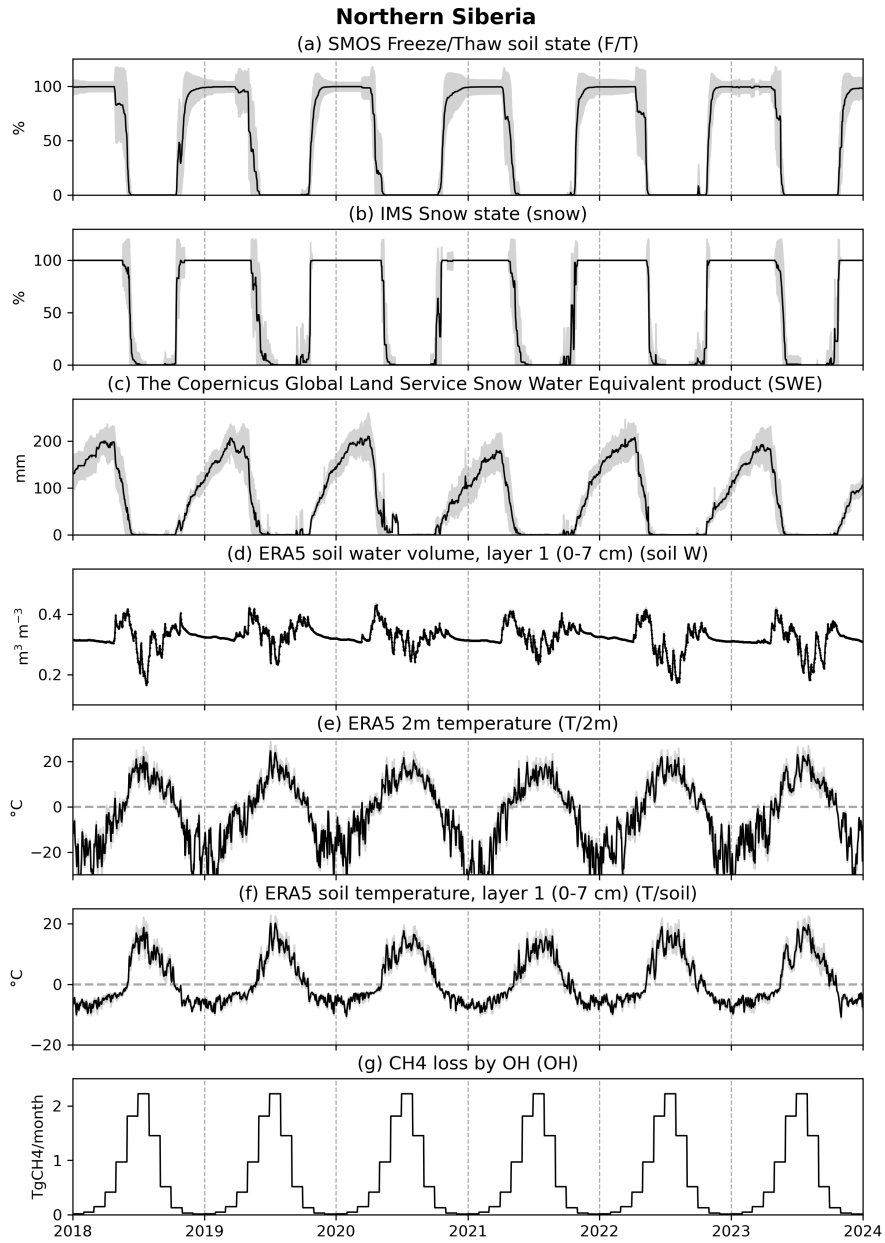
Figure C3. Black line shows the daily mean and the filled grey area the standard deviation of (a) soil freeze-thaw state, (b) snow cover state, (c) snow water equivalent, (d) layer 1 soil water volume, (e) 2 meter air temperature, (f) layer 1 soil temperature and (g) CH$_4$ loss by OH for Northern Siberia.
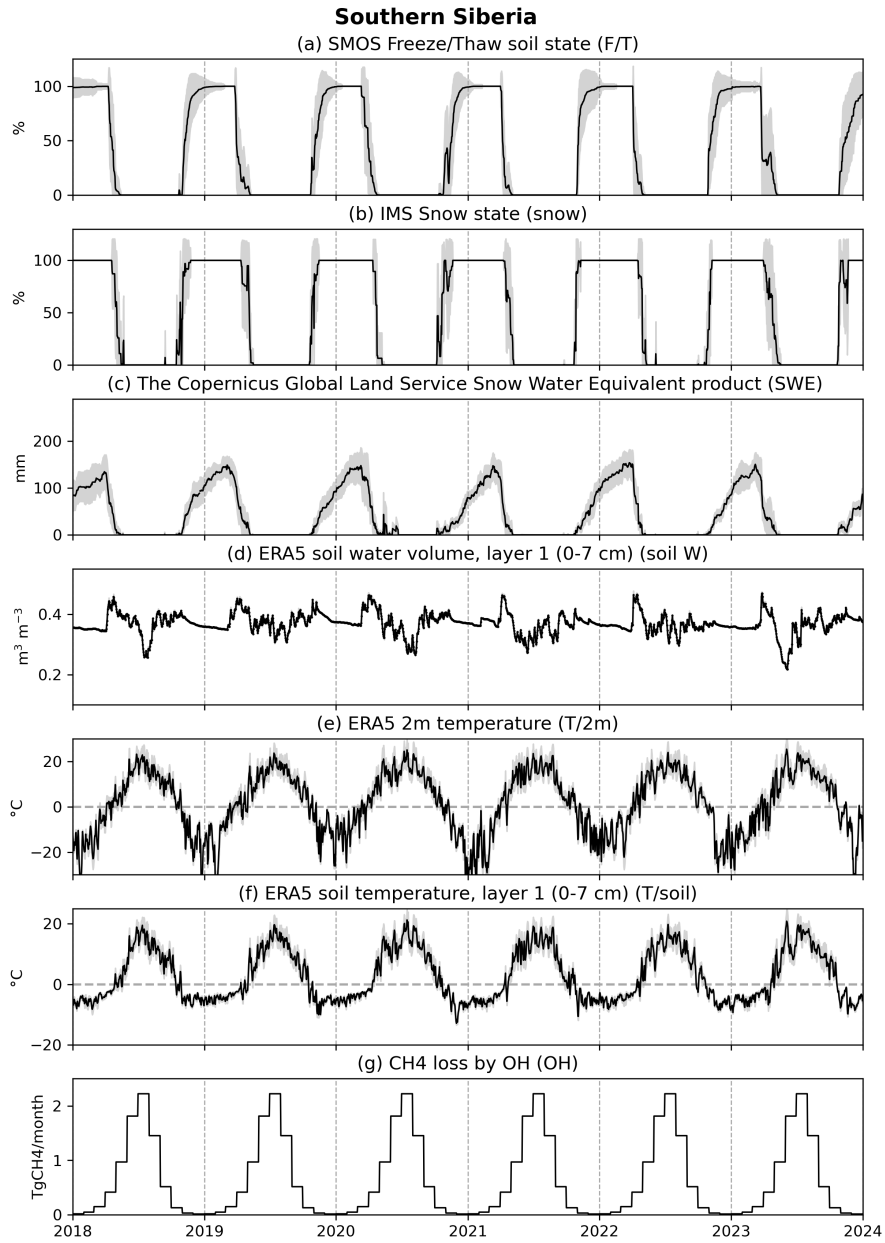
Figure C4. Black line shows the daily mean and the filled grey area the standard deviation of (a) soil freeze-thaw state, (b) snow cover state, (c) snow water equivalent, (d) layer 1 soil water volume, (e) 2 meter air temperature, (f) layer 1 soil temperature and (g) CH_4 loss by OH for Southern Siberia.

1020   **Appendix D: Day of year time series**
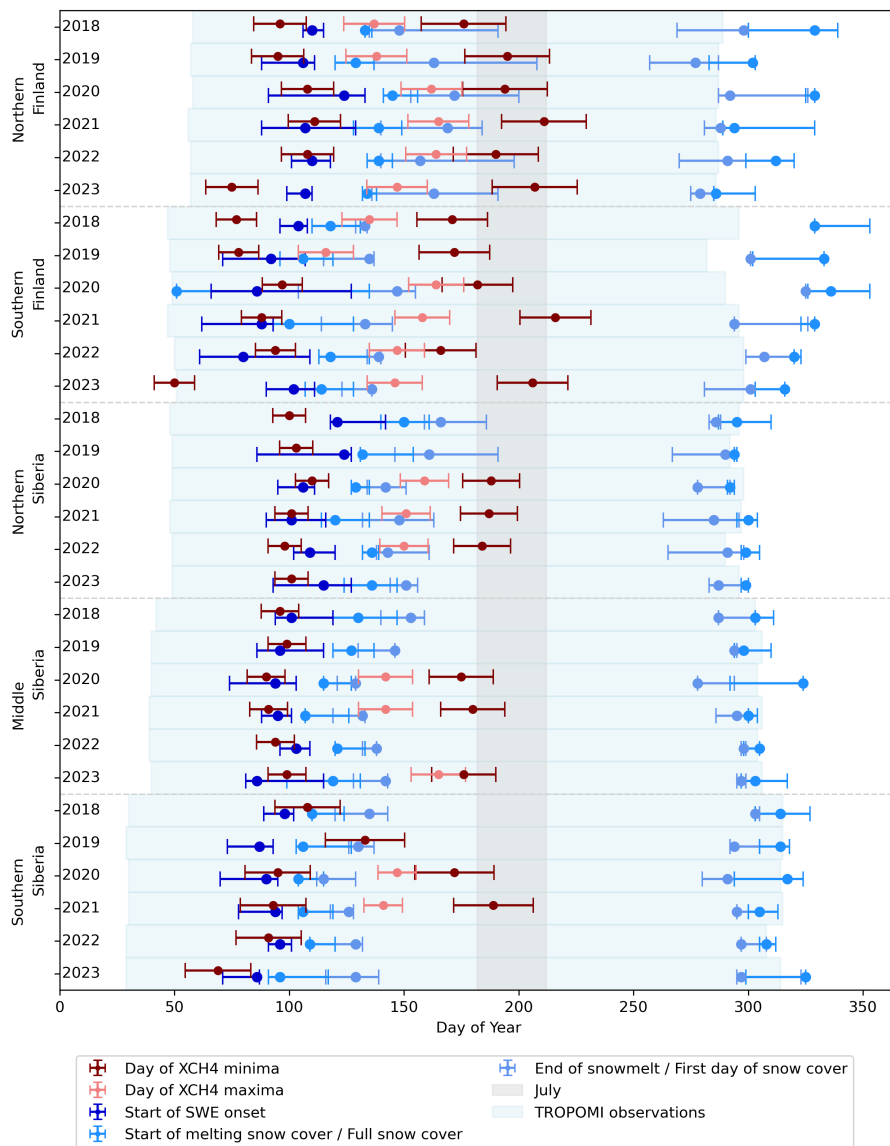
Figure D1. ~~Snow melt~~ Timing of seasonal events related to snow cover and XCH_4 minima and maxima for different case study areas and years. The markers indicate the day of year of the XCH_4 seasonal cycle minima (dark red circles), seasonal cycle maxima (light red circles), start of SWE onset (dark blue circles), beginning of snowmelt or onset of full snow ~~accumulation~~cover (first day when snow cover fraction falls below or exceeds 0.9; medium blue circles), and the end of snowmelt or start of the new snow season (first day ~~XCH~~when snow cover fraction falls below or exceeds 0.1; light blue circles). Horizontal bars denote the uncertainty in the timing, and each region-year pair is plotted as a horizontal row. The shaded gray area marks the month of July, when CH_4 ~~minimas anx maximas time series~~loss due to OH is at its maximum, and the blue background shading indicates the TROPOMI/WFMD observation period for each year.

. E.K. and H.L. participated on the conceptualization of the study. E.K. prepared and performed the data processing, analysis, original draft preparation and the visualizations for the manuscript. H.L. participated in the draft preparation and supervision. T.A., J.T., and J.P. advised in the analysis, A-M. S. advised on the analysis of OH sink, and M.T. advised in the CTE-CH$_4$ analysis. M.T. did the CTE-CH$_4$ model simulations and wrote its data description A.T. processed the CH$_4$ loss by OH data and wrote its data description. K.R. provided the SMOS F/T data. K.L. provided the SWE data. M.B. and O.S. provided the TROPOMI WFMD data. All authors read and provided comments on the manuscript.

. The authors declare that they have no conflict of interest.

. FMI team acknowledges funding from the European Space Agency projects MethEO (4000125046/18/I-NB), MethaneCAMP (4000137895/22/I-AG), AMPAC-Net (AO/1-10901/21/I-DT), SMOS L3 Freeze/Thaw L3 Data Service (4000124500/18/I-EF), and ESA SMOS ESL2020+ (4000130567/20/I-BG).

In addition, FMI team acknowledges funding from the Research Council of Finland, through WINMET project (350184), ACCC - Flagship of The Atmosphere and Climate Competence Center (357904), FAME - Flagship of Advanced Mathematics for Sensing, Imaging and Modelling (359196), and The Centre of Excellence of Inverse Modelling and Imaging (353082).

E.K. acknowledges funding from the Tiina and Antti Herlin Foundation (Projects 20180222 and 20190003).

K.R. acknowledges funding from the Research Council of Finland Academy, through Research Fellowship project EMonSoil (364034).

M.T. acknowledges funding from EU HORIZON, through IM4CA and EYE-CLIMA (101081395), and from the Research Council of Finland Academy, through GHGSUPER (351311), CHARM and FIRI-ICOS (345531).

The University of Bremen team acknowledges funding from ESA via project GHG-CCI+ (ESA contract no. 4000126450/19/I-NB) and the ~~Bundesministerium für Bildung und Forschung~~ German Federal Ministry of Research, Technology and Space (BMFTR) within its project ITMS (grant no. 01 LK2103A). The TROPOMI/WFMD retrievals were performed on HPC facilities funded by the Deutsche Forschungsgemeinschaft (grant nos. INST 144/379-1 FUGG and INST 144/493-1 FUGG).

This publication contains modified Copernicus Sentinel data (2018–~~2024~~2023). Sentinel-5 Precursor is an ESA mission implemented on behalf of the European Commission. The TROPOMI payload is a joint development by ESA and the Netherlands Space Office (NSO). The Sentinel-5 Precursor groundsegment development has been funded by ESA and with national contributions from the Netherlands, Germany, and Belgium.

We thank the team behind the LPX-Bern DYPTOP v1.4 for providing the CH$_4$ emission estimates. In addition, we thank Lena Höglund-Isaksson for providing the GAINS estimates and Antti Leppänen for providing the JSBACH-HIMMELI estimate as part of the EU-Horizon EYE-CLIMA project.

The authors would like to thank the ICOS and ICOS-Finland PIs for providing the data on CH$_4$ mole fractions. We thank the Finnish Meteorological Institute (PAL, UTO, KMP, SOD), University of Eastern Finland (PUI) and University of Helsinki (SMR) for providing the methane data in Finland. We are grateful for CSIRO Oceans and Atmosphere, Climate Science Centre (CSIRO), Environment and Climate Change Canada (ECCC), the Hungarian Meteorological Service (HMS), the Institute for Atmospheric Sciences and Climate (ISAC), the Institute on Atmospheric Pollution of the National Research Council (IIA), the Institute of Environmental Physics, University of Heidelberg (IUP), Laboratoire des Sciences du Climat et de l'Environnement (LSCE), Lawrence Berkeley National Laboratory (LBNL-ARM), the

1055 Environment Division Global Environment and Marine Department Japan Meteorological Agency (JMA), the Main Geophysical Observatory (MGO), the Max Planck Institute for Biogeochemistry (MPIBGC), National Institute for Environmental Studies (NIES), Norwegian Institute for Air Research (NILU), National Oceanic and Atmospheric Administration Earth System Research Laboratories (NOAA ESRL), the Pennsylvania State University (PSU), Swedish University of Agricultural Sciences (SLU), the Swiss Federal Laboratories for Materials Science and Technology (EMPA), Umweltbundesamt Germany/Federal Environmental Agency (UBA), Umweltbundesamt Austria/Environment

1060 Agency Austria (EAA) as the data provider for Sonnblick, University of Bristol (UNIVBRIS), University of Exeter (Univ. Exeter), and University of Urbino (UNIURB) for performing high-quality CH_4 measurements at global sites and making them available through the Global Atmosphere Watch - World Data Centre for Greenhouse Gases (GAW-WDCGG) and personal communications.

We used an AI language model (ChatGPT) to ~~support correcting the grammar of this manuscript~~ assist with grammar corrections in this manuscript and to support the adjustment of figure parameters in Python.